Addis Ababa University

Addis Ababa Institute of Technology

Center for Ethio-Mines Development

Grindibility and breakage characteristics of Sekota iron ore deposit in Wag-Himra Zone, Northern Ethiopia

A final project research submitted to the Center for Ethio-Mines Development, Addis Ababa Institute of Technology in Partial Fulfillment of the Requirements for the Degree of Master of Engineering in Mineral Engineering.

By:

Yohanes Belachew

Dr. Bogale Tadesse (Advisor)

Birtukan Yenealem (Co-advisor)

Addis Ababa, Ethiopia

June, 2023

Approval

This serves as confirmation that ***Yohanes Belachew*** *is the author of the project titled "****Grindability and breakage characteristics of Sekota iron ore deposit in Wag-Himra Zone, Northern Ethiopia.****" This is in accordance with university rules and guidelines, and is submitted in partial fulfillment of the requirements for the Degree of Master of Engineering in Mineral Engineering. It also satisfies standards for originality and quality.*

Signed by the Examining Committee:

Bogale Tadesse (PHD)	_____	_____
Advisor	*Signature*	*Date*
Burtkan Yenealem (MSc)	_____	_____
Co- advisor	*Signature*	*Date*
Dr.Eng Abubeker Yimam	_____	_____
Examiner	*Signature*	*Date*

Declaration

I hereby certify that the project I am submitting for the MEng. Degree at Addis Ababa University is my original work and has not previously been submitted for credit at this or any other university. I further confirm that all sources of information used in this project work have been properly cited.

Name: Yohanes Belachew

Signature: _____

Date of Submission: _____

This project has been submitted for examination with my approval as University

Advisor Name: Dr.Bogale Tadesse

Signature: _____

Date: _____

Acknowledgment

I want to thank the FDRE Minister of Mines for giving me the chance to study my master's degree at Addis Ababa University. I am really appreciative of my advisor, Dr. Bogale Tadesse, for his guidance, moral support, and helpful feedback in addition to his remarks and recommendations. To Mrs. Birtukan Yenealem, Staff of the Mineral Industry Development Institute and co-advisor of this project work, I would like to convey my gratitude.

My best wife, Mrs Messeret Chekole, deserves my sincere thanks for her continuous moral and material support as well as for giving me a child, Maramawit Yohanes.

I also want to express my gratitude to Mr. Hintsa-Selassie, a senior expert on the Chemical and Bio Engineering Laboratory Staff, for his endless help during the laboratory work.

Last but not least, I would like to thank my best friends Mr. Epheram Bogale and Wubale Nigat for their advice and support during the difficult moments in my life.

"Almighty God"

Table of Contents

List of Figures

List of Tables

List of Abbreviations and Symbols

Abbreviations

GSE: Geological Survey of Ethiopia; SGS: South Africa Geological Survey

USGS: United State Geological Survey

HPGR: High Pressure Grinding Roll; SPI: SAG Power Index

JKMRC: Julius Kruttschnitt Mineral Research Center; KG: Kinetic Grinding model

BBWI: Ball Millwork Index; RWI: Rod Work Index; BIF: Banded Iron Formation

AG: Autogenous Grinding, SAG: Semi Autogenous Grinding; SMP: Sekota Mining Private Company

PSD: Particle Size Distribution; DWT: Drop Weight Test: XRD: X-Ray Diffraction; XRF: X-Ray Fluorescence Spectroscopy; SEM: Scanning Electron Microscope;

CGS: Canada Geological Survey

Symbols

Gpr: Grindibility; wi: Bond work index; Wi: Work input, Gi: Grindibility index; P80:

Ecs: specific input energy (kWh/t); t10: size distribution 'fineness' index

A and b: impact breakage parameters; S: breakage probability

fmat: material breakage property (kg J−1 m−1); x: initial particle size(m)

Wm, kin: mass-specific kinetic impact energy (J kg−1); Wm, min: threshold energy below which breakage does not occur (J kg−1); k :successive number of impacts with the single impact energy; M: maximum t10 for a material subject to breakage (%); E_{min} :threshold energy (J kg−1)

Abstract

In this study, the influence of mill rotation speed and grinding time were investigated on Sekota iron ore grinding process in a batch mill with length 150 mm and inner diameter 150 mm. The particle size distribution of the feed was carried out by an electric sieve and the bulk feed was classified into three samples to perform the grinding test. Three distinct iron ore feed size fractions between -335mm to +0.71mm, -0.71mm to +0.15mm and -3.35 to -0.075mm separated by a series of √2 gaps were prepared. The fractions were milled at different grinding times (5, 15, 25, 35, 45 and 60 min) at 450 rpm and at different mill rotational speeds (250, 300, 350, 450 and 550 rpm) at 25 min. The mill rotation speed and grinding time affect the energy consumption, the desired grind size and the P80 of the feed size fraction. When grinding time increased from 5 to 60 min, the percentage of cumulative mass of target size increased from 8.5 to 31.1%, from 7.1 to 22.8% and from 10.6 to 26% for coarse, fine and mixed iron ore size fractions, respectively. Likewise, a significant amount of the desired grind size is produced as the grinding speed increases until the maximum critical speed is reached. For all feed size fractions, the required grind size amount (-0.075 mm) is not achieved at grinding times from 5 min to 60 min and at maximum mill rotation speed (450 rpm). The product size distribution of the three iron ore feed size fractions were also affected as the grinding time and the mill rotation speed increased from 5 to 60 min and 250 rpm to the maximum speed (450 rpm). The P80 values of all feed size fraction generally decreased both milling time and mill speed are increased from 5 to 60min and 250 to 450 rpm respectively. Unlike the P80, the energy consumption of the ball mill increases significantly as the mill speed and grinding time increase from 250 to 450 rpm and from 5 to 60 minutes respectively.

Keywords: *Grinding, Grinding time, Mill speed, Iron ore, particle size distribution.*

1. Introduction

1.1. Background of the study

After oxygen, silicon, and aluminum, iron is the fourth most abundant element in the Earth's crust and is an essential commodity for modern industry. The iron content of the Earth's crust is around 5%. The metal, which is chemically active, may be found in nature in rocks and soils together with other elements. The majority of common rock types contain iron, but it is typically uneconomical or exists in forms that are difficult to process. Iron-ore deposits usually have more than 25% Fe by weight. Iron ore mainly occurs in the form of oxide and hydroxide ores such as hematite (Fe_2O_3), magnetite (Fe_3O_4), goethite (FeO(OH)), limonite ($FeO(OH)\bullet nH_2O$), and minor carbonate and sulfide ores example; siderite ($FeCO_3$) and pyrite(FeS_2) respectively. The typical gangue minerals of iron are quartz, clay mineral (kaolinite and gibbsite), apatite, feldspar, and mica (CGS Mineral Commodity Series 7, 2012). In the study area, hematite and goethite with impurities of quartz and kaolinite are dominant ore minerals (GSE, 2020)).

Iron-ore deposits occur in many rocks, including igneous, sedimentary, and metamorphic rocks. Magnetite accumulations in mafic intrusions, and large deposits with possible magmatic-hydrothermal affinity, such as Kiruna in Sweden, are examples of igneous iron ores. However, more than 90% of global iron ores have produced from iron-rich cherty sedimentary rocks and their metamorphic or supergene derivatives (CGS Mineral Commodity Series 7, 2012).

According to the USGS mineral commodity summary (2022), the estimated global resources of crude iron ore is more than 180 billion tonnes, and iron ore resource is about 230 billion tonnes. The largest concentration of iron ore mainly occurred in banded sedimentary formations of the Precambrian age. The top five countries in the world in terms of iron ore reserve are Australia, Brazil, Russia, China and India (Figure1).As shown in the (Figure2), the production iron ore generally increased from 1870 to 2600Mt from 2010 to 2021.

Iron ore is the source of the primary iron used by the global iron and steel industries. As a result, it is critical for the production of steel, which in turn is essential to maintain a strong industrial base. The majority of iron ore (98%) is used to make steel, while the remaining 2% used in various other applications, such as powdered iron for certain types of steel, auto parts and catalysts; radioactive iron for medicine; and iron blue in paints, inks, cosmetics and

plastics(USGS,2021). The global consumption of iron ore increased from 1778 to 2250Mt from 2010 and 2021(see Figure2).

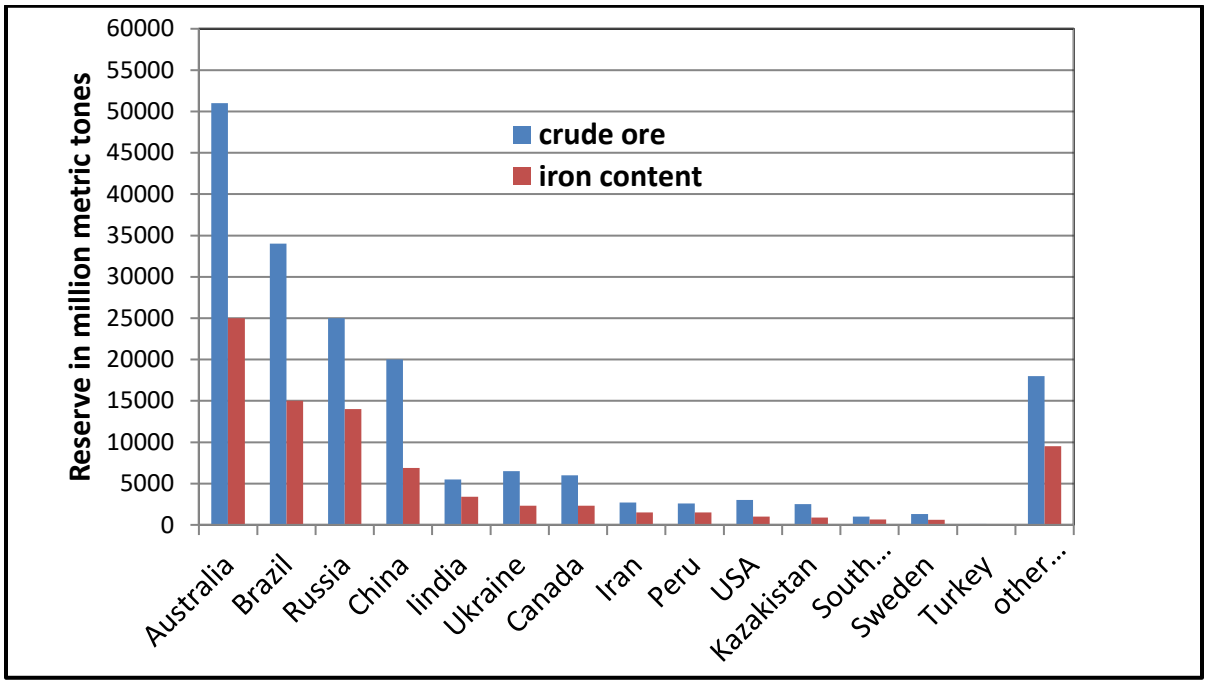

Figure 1.Global crude iron ore and iron content in 2021 by countries. Adapted from USGS Mineral Commodity summary (2022).

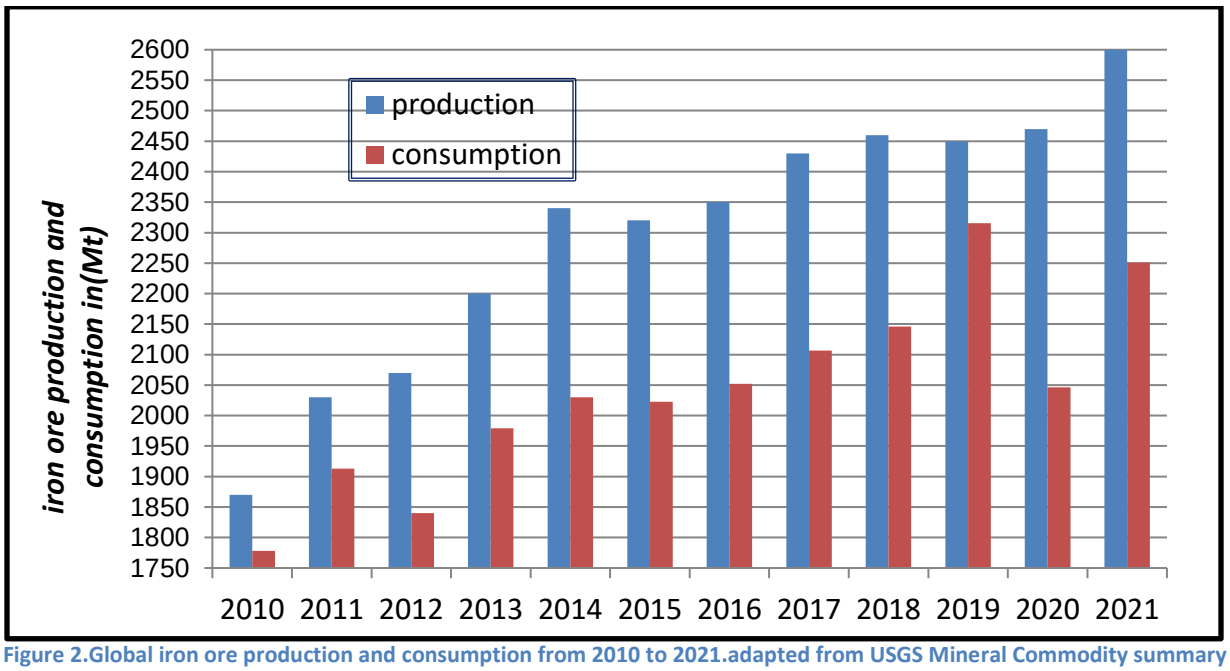

Figure 2.Global iron ore production and consumption from 2010 to 2021.adapted from USGS Mineral Commodity summary (2010-2021).

Comminution (crushing and grinding) is used to separate valuable minerals from gangue (Wills, 1990). Comminution operations are primarily based on the size of the treated particles, but composition, specific gravity, brittleness, and other properties can also influence particle comminution behavior (King, *et.al,* 2001.) The grinding stage is the final step in comminution to achieve the required size in a dry or wet medium using tumbling mills (Jankovic, *et.al*, 2015). Based on the particle size distribution and liberability of the ground ore particles, the performance of the grinding operation is designed, modeled, and evaluated (Mwanga, *et.al*, 2014). The given ore's physical breakage characteristics and grindability, in turn, have a significant effect on the product size distribution (Leung, 1987 & Hahne 2003). Moreover, these parameters also control the amount of energy needed to grind the ore mineral. According to Wills (1998), the comminution stage of the processing of ore minerals uses about 50% of the energy used overall. Therefore, to estimate the mill power requirement of a given ore mineral, a reasonable understanding of the ore grindability and breakage properties at laboratory scale is essential. As a result, many researchers have focused on the grindibility and breakage characteristics of ore minerals, such as Narayanan (1985), Tavares (2007), and Tavares and King (1998 for breakage characterization and Bond) (1962), Akande and Adebayo (2013) and Harish (2020) for grindibility of iron ore. Grindability is a term used in the industrial mineral comminution to describe the ease or difficulty of grinding an ore. This parameter measures the average grams per revolution of a tumbling mill passing 100 μm as defined by Bond (1962). However, this parameter does not consider the liberation characteristics of the relevant mineral, which are important for effective mineral separation in downstream processing (Mwanga, *et.al*, 2014).

1.2. Statement of the problem

Crushing and grinding processes known as comminution are used to separate the target minerals from the gangue Wills (1998). The final step in the comminution process is grinding, which is also one of the most crucial unit operations in the mineral processing industry. But the most energy inefficient process is grinding. More than half of the energy needed for all mineral processing operations is used during the grinding stage, while only 10 to 20 percent of the energy input is used for actual size reduction (Napier-Munn *et.al,* 2015). Grinding has therefore been a crucial area of study in the field of mineral processing due to its inefficiency.

Historically, size reduction (grinding), particularly fine grinding, for iron ore resources was not an issue due to the availability of high grade hematite ore deposits that were directly fed into the blast furnace. This deposit is now depleted, and thus cannot meet global demand. Due to the depletion of this resource and the advancement of mineral processing (i.e. size reduction, size separation, and concentration) technologies, the global community is interested in producing iron ore concentrate from low grade iron ore deposits (Hu-Chaoquan *et al.*, 2019).In these deposit liberation of valuable iron ore mineral from the gangue requires fine grinding which is the most energy intensive size reduction process. To optimize this operation, detail understanding about the grindibility and breakage characteristics of a given feed material (iron ore) is required.

In order to develop an energy-efficient grinding operation with the desired throughput, grindibility and breakage characterization studies on the low-grade iron ore deposit will gain a great attention today. The breakage characterization of different ore minerals is investigated using standard mathematical grinding models (KG and JKMRC models). These models are useful for describing and defining the grinding process. The KG model is used to demonstrate the product size distribution of various ore minerals from a given feed particle size and grinding time, whereas the JKMRC model is used to explain the relationship between input energy and product size distribution (Napier-Munn *et al*., 1996). In the present study, the grinding process of bulk iron ore was assessed based on the variation of grinding time and mill speed for different feed size. This is a newly developed approach that demonstrates how grinding time and mill speed affects, power consumption of the ball mill as well as the product size distribution and its desired grind size of a given iron ore mineral.

1.3 Objective of the study

1.3.1 Major objective

The main objective of the project is to study the grinding process, in particular the grindability and breakage characteristics of iron ore deposits that served as input for the development of grinding systems, and to provide information for selection and sizing of the grinding circuits as well as downstream mineral processing units.

1.3.2 Specific objectives

- Review the mineralogical and comminution (grinding) based studies on similar iron ore deposits and compare their result with Sekota iron ore deposit.
- Sizing crushed ores particles and characterize their effect on the grinding process iron ore
- Investigate the effect of operational parameters(grinding time and mill speed) on the grinding process of iron ore
- Identify the parameter that significantly affect the grinding process of iron ore
- Determine the grind time , mill speed and feed size for acceptable hematite liberation and desired product size distribution
- . Investigate breakage properties of the iron ore based on grinding time and mill speed variation

1.4 Scope of the study

This project was conducted by using literature review and laboratory ball mill grinding analysis. For this reason, the scope of this project work is: review of the mineralogical and grinding-based literature on various iron deposits and comparison with present studies, analysis and interpretation of textural, mineralogical and chemical results of iron deposits with respect to their grindibility and breakage properties. In addition, bacth laboratory ball mill grinding tests was carried out for three feed iron ore samples by varying grinding time and mill rotational speed. Generally, this research will be done through mineralogical characterization and laboratory ball mill grinding tests of bulk sample of Sekota iron ore deposits.

1.5. Significance of the study

I expect that this study will be useful and can give the following contributions:

- For the researcher, it is used as a motivation to conduct further study on the details of comminution behavior of Sekota iron ore deposit.
- This work is also necessary to demonstrate the amenability of the ore deposit for mining and processing companies to invest their capital.
- Finally, this research will aid in understanding how mill rotational speed and milling time affect the grinding process of the Sekota iron ore deposit.

2. Literature Review

2.1 Iron Ore Deposit

2.1.1 Deposit Types

Since iron ore deposits are known to occur in sedimentary, hydrothermal, and magmatic environments, the production of iron ore today is largely derived from these three types of deposits: about 90% of the iron ore mined comes from deposits related to Precambrian banded iron formations, and the remaining 10% comes from metasomatic skarn and magmatic magnetite deposit **(**Beukes *et.al*., 1992**)**. Various types of iron ore deposits are presented in (Table1).

Deposit type	Max.deposit size(Mt ore)	Grade (wt %)	Orebody shape	remarks	examples
Supergene/hypogene enriched BIF					
Transvaal-Hamersley type	>1.00	56-69	Sheet, lens	Predominant importance	Sishen(S/African),Serrado carajas(Brazil),Mt.tom Price(WA)
Algoma-type	<100	50-67	>>,>>,shoot	Rare type	Buhwa(zimbabwe)
Rapitan-type	<1000	50-58	>>,>>	>>	Urucum(Brazil)
Metamorphosed BIF					
taconite	>10,000	15-40	Stratiform bed	Low-grade resource	Mesabi Range(USA)
Itabirite	>1000	35-50	>> >>	not mined	Brazil, Australia
Ironstones					
Oolitic ironstones	500	25-45	Statiform bed	Not mined	Minett(Europe),canton(USA)
Reworked laterite	>1000	50-59	Channel deposit	Significant exploration potential	Robe River(Australia)
Magmatic deposits					
In mafic and ultramafic rocks	>1000	30-60	Plug,layer,irregular bodies	Not mined	Bushveld magnetite layers and plugs,Taberg(Seweden)
In alkaline complexes	2500	60-65	Massive tabular plug,dyke,flow	Regional significance	Kiruna,Gallivara,Grangesberg (Sweden)
Skarn deposits					
Magnetitic skarn	1000	40-60	Irregular mass,vein,plug	>> >>	Magnitaya Gora(Russia)
Sideritic skarn	<100	20-60	Irregular mass	>> >>	Marquesado (Spain)

Table 1.Major characteristics of important iron ore deposit types adopted from Jens Gutzmer and Nicolas J. Beukes, 1992).

2.2. Mineralogy of iron ore

2.2.1 Mineralogical analysis of iron ore

Around the world, various types of iron ores are produced. According to the USGS (2021) report, global iron ore production reached 2.4 billion tons, with Australia, Brazil, China, and India accounting for the majority. Furthermore, global iron ore reserves are estimated to be 180 billion tons, with Australia, Brazil, Russia, and China having the most reserve. The global iron ore production and reserves for 2021 is presented on (Table2).

Nation	Mine production (Thousands Metric tons)	Reserves (Million Metric tons)
Australia	900,000(1)*	50,000(1)
Brazil	400,000(2)	34,000(2)
China	340,000(3)	20,000(4)
India	230,000(4)	5,500(6)
Russia	95,000(5)	25,000(3)
South Africa	71,000(6)	1000(8)
Canada	57,000(7)	6,000(5)
United State	37,000(8)	3000(7)
World total	2,400,000	180,000

*Rankings are listed in ()

Table 2.World iron ore production and reserves (source: USGS minerals commodity summary, 2022).

Chemical composition primarily determines the quality of raw iron ores. In particular, the grade of iron ore increases with increasing total Fe content. Low levels of gangue materials and impurities also contribute to a high grade. Table3 provide information on the chemical makeup of iron ores produced in various nations (Wakelin, D, 1999; Lu, L& Ishiyama, O, 2015; Biswas, 2005; Cores, A & Babich, A, 2007; Muwanguzi and Karasev, 2012 and Song, E-x, 2013). The total Fe content is range from 31 to 69 wt%. The main gangue components in iron ore are SiO2 and Al2 O3, with concentrations ranging from 0.35 to 56 and 0.23 to 6.5 wt%, respectively. Additionally, the concentrations of sulfur and phosphorus range from 0.001-0.3 and 0.004-0.87 wt%, respectively.

		Chemical composition (mass %)						
mine	nation	Total Fe	SiO2	Al2O3	S	P	TiO2	Ref.
Goldsworthy	Australia	63.2	4.9	1.6	-	0.035	-	Biswas(2005)
Goldsworthy	Australia	62.8	6.1	1.5	0.028	0.004	0.1	Wakelin, D.H(1999)
Hammersley	Australia	62.7	4.21	2.57	0.015	0.071	0.13	Wakelin, D.H(1999)
Hammersley	Australia	62.7	4.2	2.73	0.016	0.059	-	Cores, A and Babich, A.(2007)
Mt.Newman	Australia	62.5	5.6	2.6	0.007	0.069	0.11	Wakelin, D.H(1999)
Marra mamba	Australia	61	3.3	1.8	0.039	0.069	0.07	Wakelin, D.H(1999)
Mning Area C	Australia	60.8	4.48	2.46	0.025	-	0.002	Junwoo,Park & Eunjiu. Kim,2021
Yandi	Australia	59.5	5.03	1.25	0.013	0.39	0.05	Wakelin, D.H(1999)
Yandi*	Australia	56.92	6.06	1.53	0.092	-	0.095	Junwoo,Park & Eunjiu. Kim,2021
Irvine island	Australia	54.4	21.3	0.23	0.04	0.01	-	Muwanguzi and Karasev (2012)
Itbira	Brazil	68.9	0.35	0.6	0.010	0.03	-	Biswas(2005)
MBR	Brazil	68.3	1.3	0.9	0.005	0.03	0.04	Wakelin, D.H(1999)
MBR	Brazil	67.3	0.79	0.72	0.005	0.030	-	Cores, A and Babich, A.(2007)
Carajas	Brazil	67.2	0.6	0.94	0.01	0.037	0.03	Wakelin, D.H(1999)
Carajas*	Brazil	65.61	1.77	0.91	0.011	-	0.088	Junwoo,Park & Eunjiu. Kim,2021
Carajas	Brazil	65.4	1	1.05	0.010	0.038	-	Muwanguzi and Karasev (2012)
Robe river	Canada	57.2	5.6	2.75	0.028	0.04	0.22	Wakelin, D.H(1999)
Carol lake	Canada	64.7	3.9	1	-	0.005	-	Biswas(2005)
Nanfen	China	63.4	6.28	1.17	0.110	-	-	Lu, L& Ishiyama, O(2015)

Exi	China	42.6	22.32	2.7	0.03	0.87	0.87	Song, S. and Campos-Toro, E.F(2013)
Guanzhuang	China	38.7	11.6	-	0.11	0.42	-	Lu, L& Ishiyama, O(2015)
Panzhihua	China	33	-	-	-	-	11	Lu, L& Ishiyama, O(2015)
Qidashan	China	31.2	56	-	0.3	<0.03	-	Muwanguzi and Karasev (2012)
Bailadila	India	64	2.5	2.5	0.05	0.1	-	Muwanguzi and Karasev (2012)
Donimalia	India	63.5	3	3	0.05	0.08	-	Muwanguzi and Karasev (2012)
Goa	India	57.8	2.5	6.5	0.02	0.04	-	Biswas(2005)
Bakal	Russia	60.7	2.4	2	0.03	0.004	-	Biswas(2005)
Tula	Russia	52.2	10.1	1.25	0.100	0.6	-	Muwanguzi, and Karasev(2012)
Reserve Pellet	USA	63	8.1	0.4	0.003	0.025		Biswas(2005)
Mesabi	USA	57.5	10.1	0.7	0.01			Biswas(2005)
Minnesota	USA	54.3	6.8	0.4	-			Biswas(2005)
Nyamiyaga	Uganda	69	0.62	0.43	0.001			Muwanguziand Karasev(2012)
KyanyamuzInda	Uganda	68.7	0.41	0.35	0.006			Muwanguzi and Karasev (2012)
Rushekye	Uganda	67.9	0.96	0.58	<0.001			Muwanguzi and Karasev (2012)
Sekota	Ethiopia	36.09	30.11	9.25	-	--	-	GSE(2020)
Bikila	Ethiopia							
Mekane Selam	Ethiopia	33.62	30.3	12.3	-	0.1		GSE(2020)

Table 3. Shows chemical composition of iron ores in different nations.

A comparison of the chemical make-up of iron ores from various nations is shown in Figure3. Brazil, Canada, and Uganda all have high-grade iron ores with total Fe contents that exceed 60 weight percent (Geerdes.M &Toxopeus.H, 2009). The ore grade is roughly 60 weight percent in Australia, India, the United States, and Russia. Aside from frequently having high SiO2, phosphorus, and sulfur contents, iron ores from China in particular have a disadvantage in terms of the total Fe content. Chinese iron ores may also contain TiO2, which could lead to the formation of TiC (Titanium Carbide) in operating blast furnaces (Liao, Wang and Zhang, 2012).

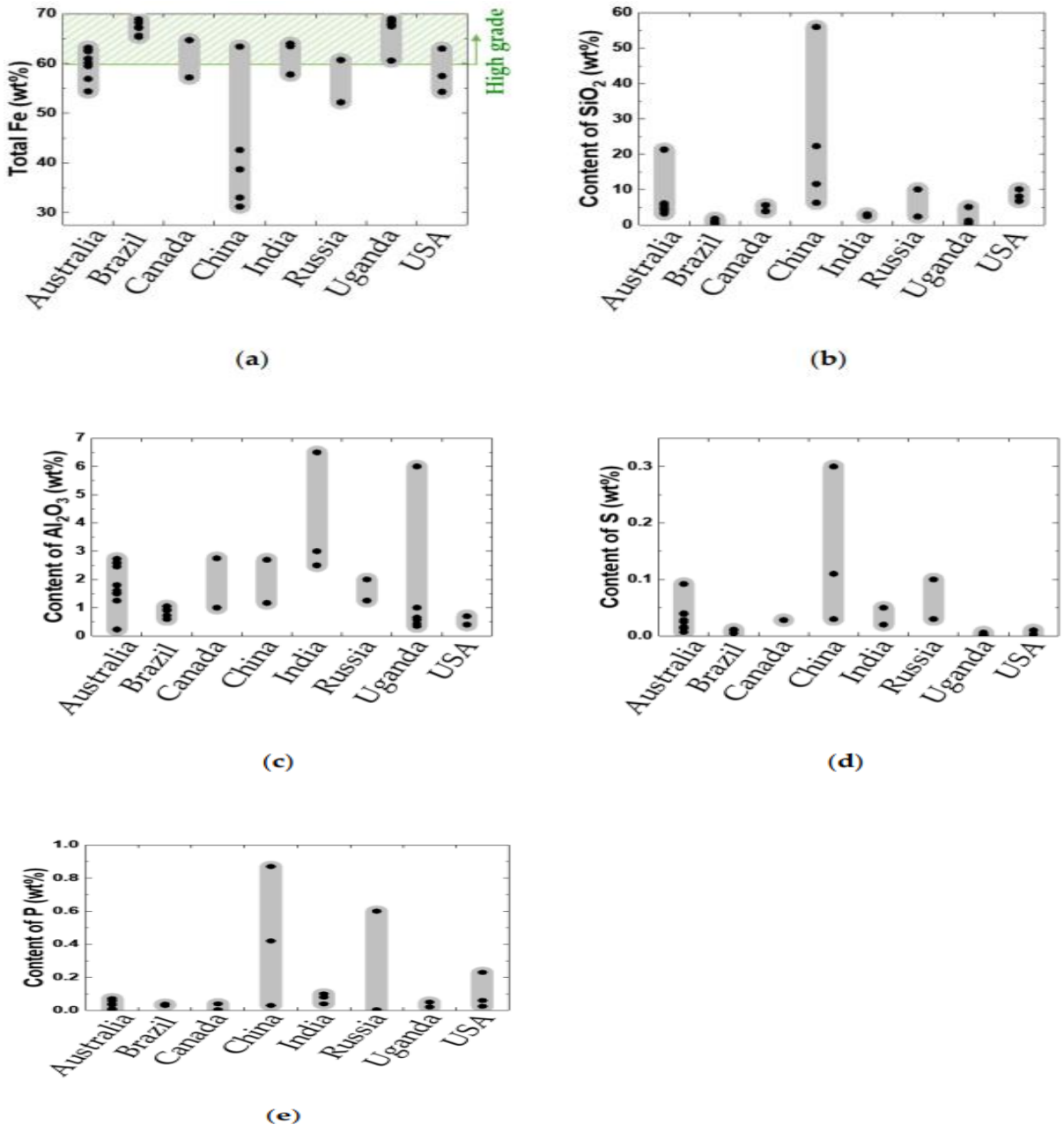

Figure 3. Comparison of chemical compositions of iron ores in different nations: (a) Total Fe, (b) SiO2 , (c) Al2O3 , (d) S, and (e) P content.

Iron ore is made up of different mineral phases that fall under the ore and gangue mineral categories. Table 4 provides a summary of typical ore and gangue mineral phases. A few well-known ore minerals include hematite, magnetite, and goethite. Gangue materials like quartz, kaolinite, and gibbsite are primarily composed of SiO2 and Al2O3.

Chemical Formula			
Ore Minerals		**Gangue Minerals**	
Hematite	Fe_2O_3	Quartz	SiO_2
Magnetite	Fe_3O_4	Kaolinite	$Al_4(Si_4O_{10})(OH)_8$
Goethite	FeOOH	Gibbsite	$Al(OH)_3$
Maghemite	$Fe^{3+}[Fe^{3+}{}_{1.67}[$ $]_{.33}]O_4$	Minnesotaite	$(Mg,Fe)_3Si_4O_{10}(OH)_2$
Kenomagnetite	$Fe_{3-x}(\ )_xO_4$	Stilpnomelane	$(K,NA,Ca)_{0.6}(Mg,Fe^{2+},Fe^{3+})_6$ $Si_8Al(O,OH)_{27}2\text{-}4H_2O$
Hydrohematite	$Fe_{(2-x)/3}(OH)_xO_{3-x}$	Chlorite	$(Fe,Al,Mg)_3(Si,Al)_2O_5(OH)_4$
		Pyrite	FeS_2
		Pyrolusite	MnO_2
		Siderite	$FeCO_3$
		Ankerite	$Ca(Fe, Mg, Mn)(CO_3)_2$

Table 4.Common ore minerals and gangue mineral phases in iron ore (Lu.L&Ishiyama.O, 2015).

2.2.2 Textural analysis of iron ore minerals

According to their texture and iron content, iron ores are divided into five categories: granular-hematite, specular-hematite, massive hematite, hematite-magnetite, mylonitic hematite, and magnetite (Fig 4). The grindability and breakage characteristics of ore minerals are significantly influenced by texture. As a result, grindability is higher for ore types with coarse-grained iron oxides and straight grain boundaries than for fine-grained ore types with irregular-to-no visible grain boundaries (M.K. Togersen, *et al*., 2018).

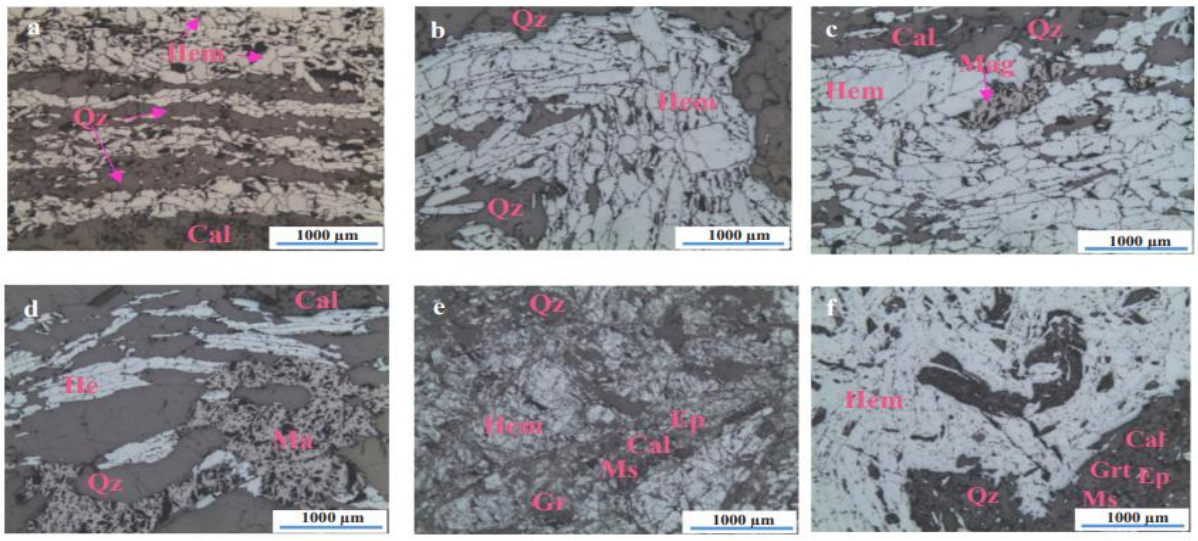

Figure 4. Reflected light photomicrographs showing typical hematite texture in the different ore types. (a) Granular-Hematite, (b) Specular-Hematite, (c) Hematite-Magnetite, (d) Magnetite-Ore, (e) Mylonitic-Hematite, and (f) Massive-Hematite(Togersen, et al, 201).

Iron ore types	Description	Hardness	Grindibility
Granular-Hematite	Grain size: the average grain size of hematite was estimated to 200 µm. Grain shape:equigranular equigranular, with tabular shape, and has straight grain boundaries. Guangue:quartz,calcite	Low(624)	high
Specular-Hematite	Similar to Granular-Hematite, Specular-Hematite exhibits equigranular textures and straight grain boundaries. The average grain size of specular-hematite is between 400 and 500 µm, which sets it apart from other types of hematite. The grains of hematite are tabular, long, and parallel to the layering.	Low(576)	high
Massive-Hematite	Grian size: very fine grianed Grain shape:irregular Grain boundary is not straight.	Hard(632)	low
Hematite-Magnetite	Grian size:HM-300 µm,Mgt-1mm Grain boundary:straight to irregular. Gain shape:tabula HM,equant-irregular Mgt	Medium(648)	medium
Mylonitic-Hematite	Fine-grained (10-20 µm) hematite is typically found dispersed in a fine-grained matrix of gangue minerals. In the matrix, there are also traces of coarse-grained hematite.	Hard(711)	low
Magnetite	Grain size;0.5cm Straight to irregular grain boundary	Medium(659)	medium

Table 5. Shows the textural description of typical iron ore minerals. Adapted from (M.K. Tgersen et al., 2018).

2.3 Grinding

Grinding is the final stage size reduction process in mineral processing, and it is critical for the extraction of valuable minerals from ore. The main principles of grinding are impact and abrasion. Grinding is a highly energy-intensive size reduction method, accounting for 50% of

total energy consumption for mineral extraction (Michaud, 2016). According to the Mining Energy Consumption (2021) report, processing iron ore (magnetite) is the most energy-intensive, followed by copper and gold ores (Figure 5).

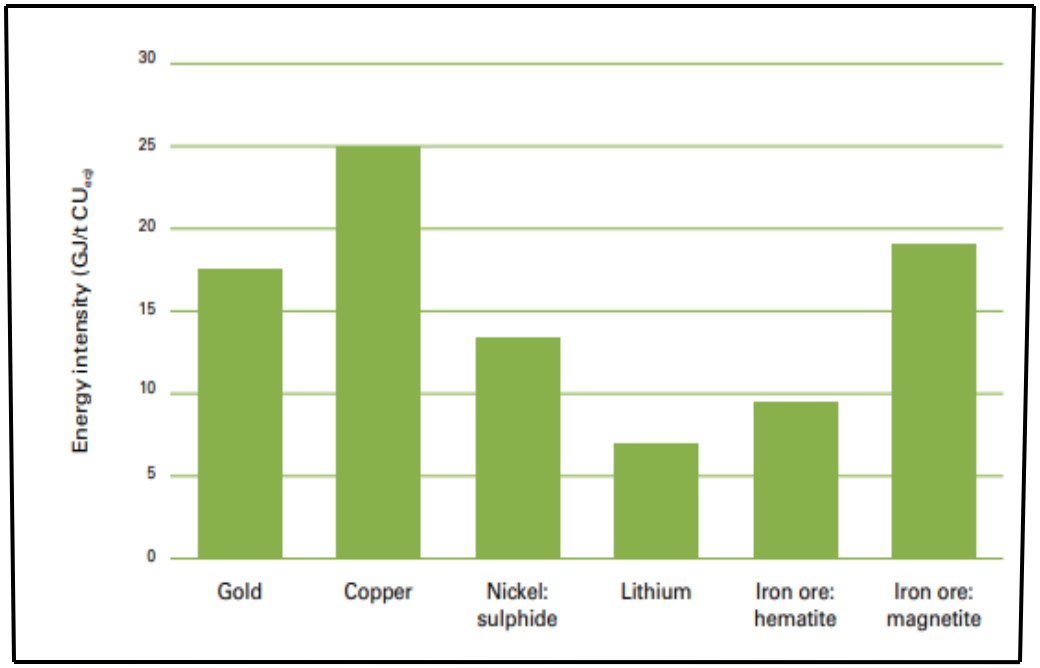

Figure 5. Grinding energy consumption of different ore minerals (source: Mining Energy Consumption 2022)

Grinding is done solely by the nipping method, and the media can be a ball or rod. The size of the media has an impact on ore properties and output quality. Milling devices used for grinding ore minerals are classified as tumbling mills or stirred mills based on the charge motion (Wills, 2006; Gross, 1938). In tumbling mills, the mill shell rotates, imparting motion to the charge (see Figure 6), and the critical speed ranges between 50 and 90%. Tumbling mills are used for coarse grinding and are classified based on the type of media used as rod mills, ball mills, AG mills, and SAG mills. The feed and product ore material sizes in tumbling mills range from 5-250mm and 40-300µm, respectively. Stirred mills, which are used for fine and ultra-fine grinding, are classified as horizontal (IsaMill) or vertical (Sala Agitated Mill) based on the orientation of the mill shell. The feed material size ranges from fine (15-40µm) to ultra-fine (15µm) (Wills, 2006).

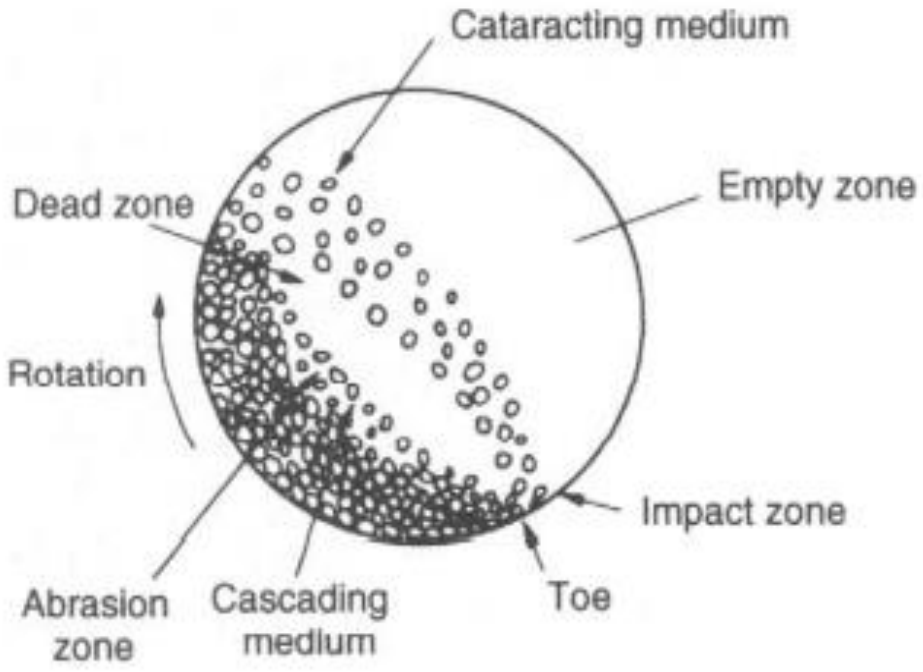

Figure 6. Motion of charge in tumbling mill (Wills, 2006).

2.4 Grindibility

Grindability is defined as the amount of material less than a specific size produced in a grinding stage divided by the net specific energy (energy used for grinding multiplied by the mechanical efficiency of the grinding device) used in that grinding stage. For grindability calculations, either 75 or 106 mm sieves can be used as the control sieve (Abdul Mwanga, Rosenkranz, & Lamberg, 2017). It is a comminution parameter that measures the average grams per revolution of a tumbling mill passing 100µm according to Bond's definition (1962).

2.4.2 Grindibility test methods

The degree of breakage (or hardness) of a given ore samples is measured by the grindibility test. Over the years, several grindability tests have been developed for different applications, each with its own strengths and weaknesses. The currently available grindibilty test methods are summarized in (Table 6) and experimental procedure of the most widely applicable grindiblity test methods in mineral processing industry are discussed below.

SMALL-SCALE TEST	TOP SIZE (mm)	CLOSING SIZE (mm)	SAMPLE REQUIREMENT[1] (kg)	TYPE	STEADY-STATE (y/n)	MILL DIAMETER (m)
Bond Ball Mill	3.3	0.149	5	Locked Cycle	Y	0.305
SAG Power Index (SPI)	19	N/A	5	Batch	N	0.305
SMC Test	22	N/A	5	Single Particle	N	N/A
Bond Rod Mill	13	1.2	10	Locked Cycle	Y	0.305
Bond Impact	75	N/A	10	Single Particle	N	N/A
Drop Weight	64	N/A	75	Single Particle	N	N/A
MacPherson Autogenous	32	1.2	100	Continuous	Y	0.45
Media Competency	165	N/A	300	Batch	N	1.83
LABWAL HPGR	12.5	N/A	25	Continuous	Y	0.25[3]

Table 6. Summary of grindability tests that are currently available to the Market for ore characterization and circuit design (source: SGS Minerals, 2005)

2.4.2.1 Bond Ball mill grindibility test

It is carried out in accordance with the original Bond procedure. It requires 10kg of material that is less than 6-mesh (3.35mm), preferably prepared at the testing facility by stage crushing the sample to 100% passing 6-mesh, but typically less than 5kg is used in the test. The test is then finished with a fine screen (typically between 65 and 270 mesh), and the screen size is typically chosen to achieve the required final product P80. The test is run as a locked-cycle with a 250% circulating load until a steady-state is reached. The Bond work index (BWI) is determined by counting the number of new grams per revolution (Gpr) produced during each cycle (SGS Minerals, 2005).

$$BW_i = \frac{44.5}{P_1^{0.23} \times Gpr^{0.82} x \left(\frac{10}{\sqrt{P_{80}}} - \frac{10}{\sqrt{F_{80}}} \right)} \quad (1)$$

2.4.2.2 Bond Rod mill grindibility test

The Bond Rod Mill Grindability Test is carried out in the same manner as the ball mill test. The feed sample is crushed to ½ inch (12.5mm) in stages and the test is run with a 100% circulating load. However, for AG/SAG mill analysis, the typical 14-mesh (1.18 mm) sieve is typically

used, This is similar to the ball mill test in that the test may be halted using various filter sizes (SGS Minerals, 2005). The rod mill work index is calculated using an equation very similar to the ball mill test, which is as follows:

$$RW_i = \frac{62}{P_1^{0.23} \times Gpr^{0.625} x \left(\frac{10}{\sqrt{P_{80}}} - \frac{10}{\sqrt{F_{80}}} \right)} \qquad (2)$$

2.4.2.3 JKTech Drop-weight Test

The JKTech drop-weight test has been developed in the Julius Kruttschnitt Mineral Research Center and demonstrated by Napier-Munn et al (1996), and this test is divided into three components. First, the test determines the resistance to impact breakage of coarse particles ranging in size from 63 to 13.2 mm (five fractions). Following, it evaluates the resistance to abrasion breakage of particles in the range 53 to 37.5 mm. Finally, the rock density of 20 particles is calculated to determine the average ore density and dispersion. Under various impact and abrasion breakage settings, the test creates the ore's appearance function (for example, breakage pattern), which is then condensed into three parameters: A, b (impact), and ta (abrasion). In the JKSimMet modeling and simulation package, the appearance function can be used to predict ore response comminution processes such as AG/SAG, crusher, ball mill, and HPGR. The testing facility should prepare 75 kg of material to generate 30-90 particles in five size fractions ranging from 13.2 to 63 mm. A great number of drop-weight tests have been performed over the years, which allows for comparison between ore types in a database. The frequency distribution of 'A x b' from JKTech is presented in Figure (SGS Minerals, 2005).

In impact testing, five size fractions are subjected to three series of impact tests at different energy levels for a total of 15 series of tests. Each test series consists of 10-30 ore samples. All particles in each series are impacted with a known energy level with a given height and weight of the drop weight head. Fragments from all test suites are collected and then subjected to particle size analysis. This reduces to a family of normalized't' values representing size reduction. The t-value is defined as the percentage of fragment weight that exceeds 1/t of the original size.

$$t_{10} = A(1 - e^{-b \cdot Ecs}) \ldots \ldots \ldots \ldots \ldots \ldots \ldots \ldots (3)$$

For the AG/SAG mill model, the t10 values are reduced to two parameters, the A and the b, using the equation below. According to SGS Minerals (2005), the model's parameters are A and b, and Ecs is the specific energy of comminution in kWh/t.

A 3-kg sample of 53 x 37.5-mm ore is used in the abrasion test. The sample is grind for 10 minutes in a 30 cm x 30 cm tumbling mill and then the product is being subjected to a size analysis. Another interesting aspect of the drop weight test procedure is that it provides a measurement of the variation in rock hardness by size, ranging from 13.2 mm to 63 mm (SGS Minerals, 2005).

2.4.2.4 SAG Power Index (SPI) Test

John Starkey (1996) created the SAG power Index, which is now offered by MinnovEX Technologies Inc.SPI, expressed in minutes, is defined as the time (t) required to reduce an ore sample from 1/2 inch F80 to 1.7 mm P80. Batch testing is conducted on a 12 inch diameter by 4 inch long laboratory mill with a 15% charge of 1 inch diameter steel balls. It needs 2 kg of ore with a top size of 3/4 inch (19 mm). SPI has the advantage of being lightweight (5 kg), which makes it suitable for geological mapping of deposits. The SPI test has been widely used in recent years to compare mineral deposits submitted for research against databases of hardness and variability (SGS Minerals, 2005).

2.5 Ore Breakage Characteristics

2.5.1. Types of Breakage Mechanism

In industrial comminution devices like tumbling mills, particle size reduction happens through three basic mechanisms: impact, abrasion, and attrition (Wills & Napier-Munn, 2006).

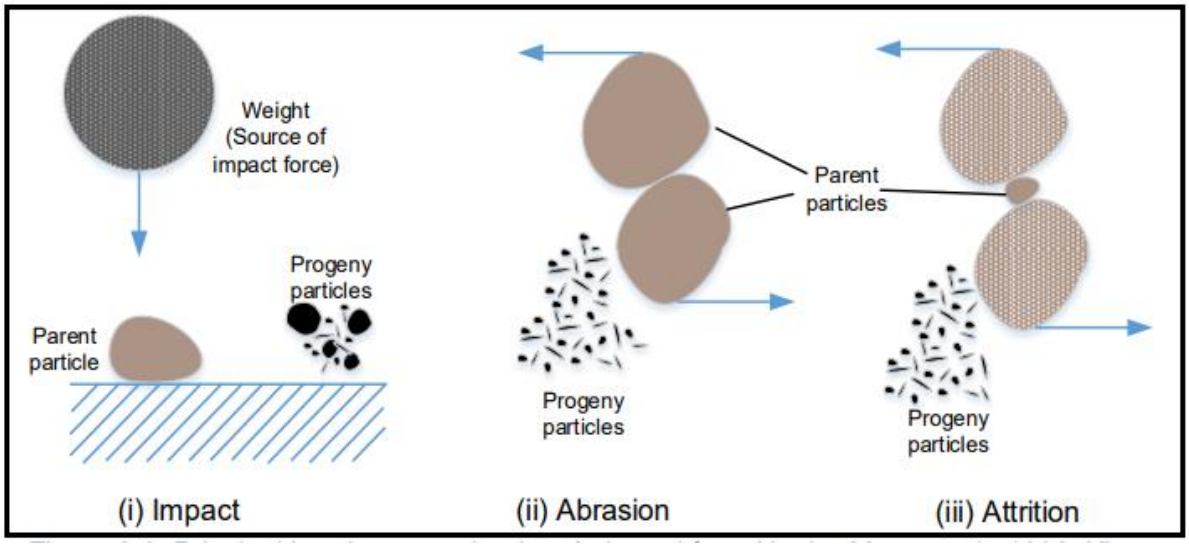

Figure 7.Principal breakage mechanism (adapted from Napier-Munn et al., 1996; King, 2001)

2.5.2 Ore Breakage Characterization

Ore breakage characterization is the process of evaluating how particulate materials fracture in comminution apparatuses, such as crushers or tumbling mills (Napier-Munn *et al*., 1996). It produces parameters that are used to describe the resistance of particles to breakage (hardness). The comminution circuit's ore feed is made up of a variety of ore types with various properties (Hahne *et al*., 2003). Therefore, ore breakage characterization enables to reveal of the various ore types, in terms of their hardness, within the feed being supplied to the comminution circuit.

The throughput of comminution devices fluctuates as a result of variations in ore properties or the mixing of different ore types obtained from various sources (Williams & Holtzhausen, 2001). These changes, in turn, affect how these devices estimate their energy needs and product attributes (Hahne et al., 2003).These changes therefore have an effect on how these devices estimate their product attributes and energy needs (Hahne et al., 2003). This has increased the importance of ore breakage characterization (Bourgeois & Banini, 2002), especially in optimizing comminution processes.

2.5.3 Effect of Parameters on the Resultant Breakage

2.5.3.1 Effect of input energy on the degree of breakage

Input energy has been revealed as the prominent controlling factor of the product size distribution from single-particle breakage in comminution processes (Tavares, 2007). Kick (1885) noticed that the volume of material broken was directly related with input energy and proposed a different energy-size reduction relationship. In addition, Tavares (2007) indicated that as input energy rises, so does the stressing intensity, which ultimately speeds up the propagation of cracks in a material. As a result, increased input energy usually increases the degree of breakage (Narayanan, 1985; Kapur *et al*., 1997; Banini, 2000; Shi & Kojovic, 2007). Nevertheless, by continuously increasing the stressing energy until a maximum product size distribution is attained, particles of infinite fineness could not be generated in a single loading event (Napier-Munn et al., 2004).

2.5.3.2 Effect of feed particle size on the degree of breakage

The particle size effect on the degree of breakage has been investigated largely in works such as Tavares and King (1998), Banini (2000), Shi and Kojovic (2007). Tavares and King (1998) showed that the ability of a particle to resist a stress without fracturing (particle strength) increases with a decrease in particle size. Because of this, larger mineral particles tend to provide low degree of breakage and thus easier to break than smaller particles. These results were also ascertained by Banini (2000) as well as Shi and Kojovic (2007). This trend is because the fracture density of larger particles is much higher than that for smaller particles (Tavares & King, 1998).

2.5.4 Standard breakage characterization models

Models for breakage or hardness characterization use mathematical relationships to represent the relationship between input energy and product size distribution (Napier-Munn et al., 1996). A single curve containing the breakage performance of various materials can be used to describe the breakage probability of different materials (Vogel & Peukert, 2004). This information is helpful in forecasting the efficiency of comminution devices (Morrell et al., 1996; Bueno et al., 2013).

2.5.4.1 t10 Breakage Model

An appearance or breakage distribution function was developed by Leung (1987). This is an explanation of how an ore particle in an AG/SAG mill breaks when energy is applied to it (Morrell *et al.,* 1996). According to Leung (1987), the relationship between the specific input energy (Ecs) and the degree of breakage (t10 parameter), which is measured as the percentage of material passing 1/10th of the initial feed size, is not linear as proposed by Narayanan (1985) but rather exponential(see equation 4).

$$t_{10} = A(1 - e^{-b \cdot Ecs}) \ldots\ldots\ldots\ldots\ldots\ldots\ldots\ldots\ldots\ldots (4)$$

This equation is also used in JKSimMet (Mineral Processing Simulator, a software package used in the mining industry) to analyze and predict AG/SAG mill performance (Schwarz & Richardson, 2013; Morrison & Richardson, 2002). The impact breakage parameters, A and b, characterize the fragmentation behavior of the material and can be determined by interpreting the typical t_{10}-Ecs curve shown in Figure8 (Tavares et al., 2007).

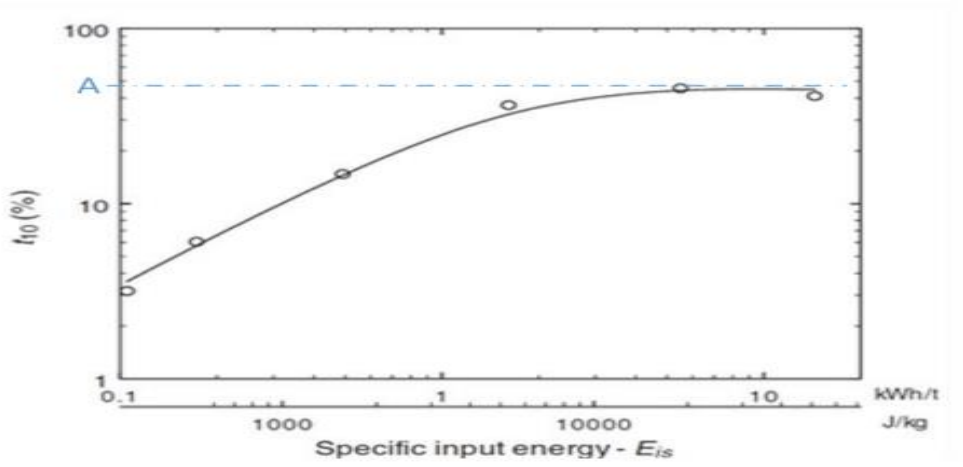

Figure 8. Relationship between the parameter t10 and specific input energy (Tavares et al., 2007).

The value of parameter A corresponds to the ore's maximum degree of breakage (t10). It suggests that as the specific input energy increases, little or no size reduction occurs at higher energies. At energies less than 1 kWh/t, parameter b is the linear gradient of the curve and is related to material stiffness (Napier-Munn et al., 1996). The slope of the curve at 'zero' input

energy, as determined by equation 5, is also significant. When an equation 4 is differentiated with respect to Ecs, the result is:

$$\frac{dt_{10}}{dEcs} = (-Ae - b \cdot Ecs) \cdot (-b) \quad \ldots\ldots\ldots\ldots (5)$$

Assume Ecs is approach to the zero, and then result will be:

$$\lim_{Ecs \to 0} \left(\frac{dt10}{dEcs}\right) = \text{A} * \text{b} \ldots\ldots\ldots\ldots\ldots (6)$$

The slope of the curve at 'zero' input energy is shown in Equation (6). It denotes a material's susceptibility to fragmentation through impact (ore hardness indicator) (Shi & Kojovic, 2007. A greater Axb value denotes that the ore type is ready to fracture, whereas a lower Axb value shows that the ore is very resistant to impact breakage (Hahne et al., 2003).The JK Drop weight tester at the JKMRC was used to determine the typical ore hardness classes listed in (Table7).

Property	Very Hard	Hard	Mod. Hard	Medium	Mod. Soft	Soft	Very soft
A*b	<30	30-38	38-43	43-56	56-67	67-127	>127

Table 7.Reported ranges of Axb values impact breakage parameters (Napier-Munn et al., 1999).

2.5.4.2 Size Dependent Model

Vogel and Peukert(2004) established a breakage probability that depends on the mass-specific impact energy, the minimum energy needed to fracture any particle, the initial particle size, and a material parameter that describes the material-specific breakage behavior. This model uses a set of parameters from equation 7 to express the breakage probability (S).

$$S = 1 - \exp\{-fmat.\, x.\, k\,(Wm,kin - Wm,min)\} \ldots\ldots\ldots\ldots\ldots\ldots (7)$$

,

Wm,kin (J kg−1) the mass-specific kinetic impact energy,

Wm, min (J kg−1) the threshold energy below which breakage does not occur, and

k the successive number of impacts with the single impact energy.

To describe the degree of breakage, t10 (%), in relation to material property, particle size, and net cumulative impact energy, the Vogel and Peukert's breakage probability model is modified (Shi & Kojovic, 2007).The new model equation is given as follow:

$$t10 = M\{1 - exp[-fmat.\ x.\ k\ (Ecs - Emin)]\} \ \ldots\ldots\ldots\ldots\ldots\ldots (8)$$

This model was directly compared to the t10 breakage model (equation), in which the value of A was replaced by M, b by fmat.x, and Ecs by k. (Ecs-Emin).

Shi and Kojovic (2007) used the data from Mt Coot-tha quarry material to fit both the t10 breakage model (equation4) and the size dependent model (equation8).

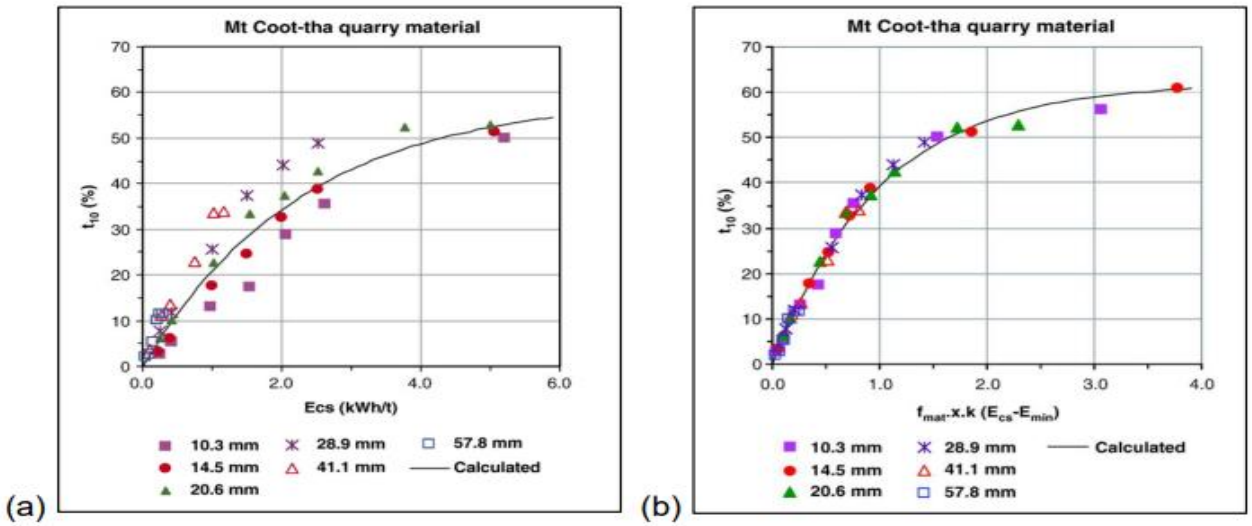

Figure 9. Example of (a) t10 against Ecs and (b) t10 against fmat.x.k (Ecs-Emin) curves (Shi & Kojovic, 2007).

The plots in Figure 2.4 (a) and (b) demonstrate that the two models predict the same maximum value for t10 (roughly 60%). However, compared to the t10 breakage model, the size dependent model more closely matches all of the data sets.

2.5.4.3 Kinetic Grinding model (KG model)

KG model (i.e. population balance model) is developed by (Austin, L.G&Luckie, P.T, 1972) and (Reid, K.G., 1965). Numerous research have used the fundamental ideas behind the models to describe the breakage rate and breakage distribution in ball mills while grinding different materials with different operating factors (Austin, L.G., 1999; Kwon, J., 2012, 2014&2016). In a KG model, the breakage process is divided into the breakage rate function and the breakage distribution function. These two functions are primarily influenced by the material properties,

mill size, and operating conditions. They are typically identified in a laboratory using a series of breakage tests with single-sized feeds.

The breakage rate function is determined by separating feed particles by using radical two sieve fractions. To test the breakage kinetics, a single size fraction is ground for a predetermined period of time. Following that, the percentage of ungrounded particles is measured.

For the sample, which MinnovEX prepared to have a F80 of 13mm. For the purpose of obtaining time-series data, grinding and sieving are repeatedly performed with variable grinding times. The time-series data is then used to calculate the estimated breakage rate for the specified size fraction.

The breakage function can be determined by measuring the breakage rates for a wide range of particles with single size fractions, which is a time-consuming process. To use the breakage functions from laboratory-scale experiments in an industrial grinding circuit, it must be corrected. To establish correlations between lab-scale and industrial mills, empirical equations are used to determine the dependence of breakage parameters on ball/mill dimensions and operating parameters (Austin, L.G& Klimpel, R.R., 1984).

3. Materials and Methods

3.1 Iron ore sample

3.1.1 Overview

The iron ore samples were taken from Sekota iron ore deposit. Sekota iron ore deposit is located in the northern part of Ethiopia, specifically in North Eastern part of Tekeze basin. The accessibility and location of the deposit area in relation to the surrounding area is shown in (Fig.10). According to the SMP (2016) report, the Sekota iron ore deposit is made up of two major blocks: Tsitsika and Shakura. The Tsitsika Block is located on the eastern border between Sekota and Zikwala Woredas and is bordered by Tsitsika town, the seat of Zikwala Woreda, in the west and Debrebirhan Kebele, one of the Kebeles in Sekota Woreda, in the east. It is also 35 kilometers west of Sekota, the administrative capital of the Wag-Himra Administrative Zone (Figure10). The Shakura exploration block is located in Abergele Woreda, approximately 40 kilometers north of Sekota. This block is bounded to the south by Sewir and Wana villages and to the north by Mekane Genet (Figure10).The geographic UTM coordinates of Tsitsika and Shakura blocks are shown on the (Table 8).

Block name	Corner point	Easting(m)	Northing(m)
Tsitsika	1	480,000	1,418,000
	2	487,376	1,418,000
	3	487,409	1,414,623
	4	490,831	1,414,601
	5	490,840	1,409,246
	6	487,298	1,409,243
	7	487,317	1,404,000
	8	480,000	1,404,000
Shakura	9	496,000	1,431,000
	10	502,000	1,431,000
	11	502,000	1,421,000
	12	496,000	1,421,000

Table 8.Geographic coordinates of Tsitsika and Shakura blocks at different corner point. Adapted from (SMP, 2016).

In geological speaking, the deposit area is covered by Mesozoic clastic (sandstone, mudstone, and shale) and carbonate (limestone) rocks, as well as tertiary volcanic basalts with associated pyroclastic deposits. According to SMP (2016) report, Sekota iron ore deposit is primarily composed of hematite (greater than 50%), with minor amounts of limonite and goethite (17%), and the main impurities are SiO2 (10-20%) and Al2O3 (3-10%) with low amounts of phosphorus and sulfur. The mineralized zone is classified as massive, laterite, pisolithic layer, mottled zone, and fractured zones with iron replacement.

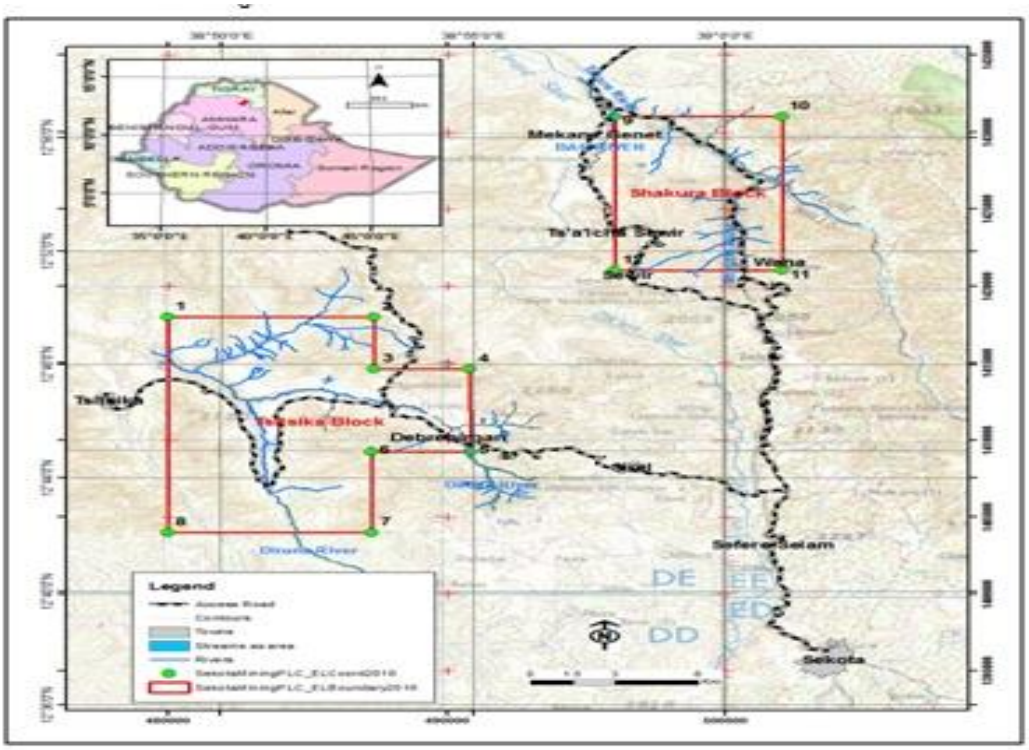

Figure 10: location map of Sekota iron ore deposit.Adaptad from (SMP, 2016)

3.1.2 Iron ore sampling

The ore is sampled based on the degree of variation in the mineralogical composition and textural properties of the ore deposit. As a result, 50Kg bulk sample was taken from Akmayohanes locality which is a part of Shakura block in Sekota iron ore deposits (Figure11). Field equipments, whether scientific or not are including; GPS, hand lens, geological hammer, base map, sample bag, note book, pencil and pen and car drive. The samples are properly labeled during sampling, and GPS readings are taken for each sample. Besides that, samples are properly packed in clean sample bags to avoid contamination.

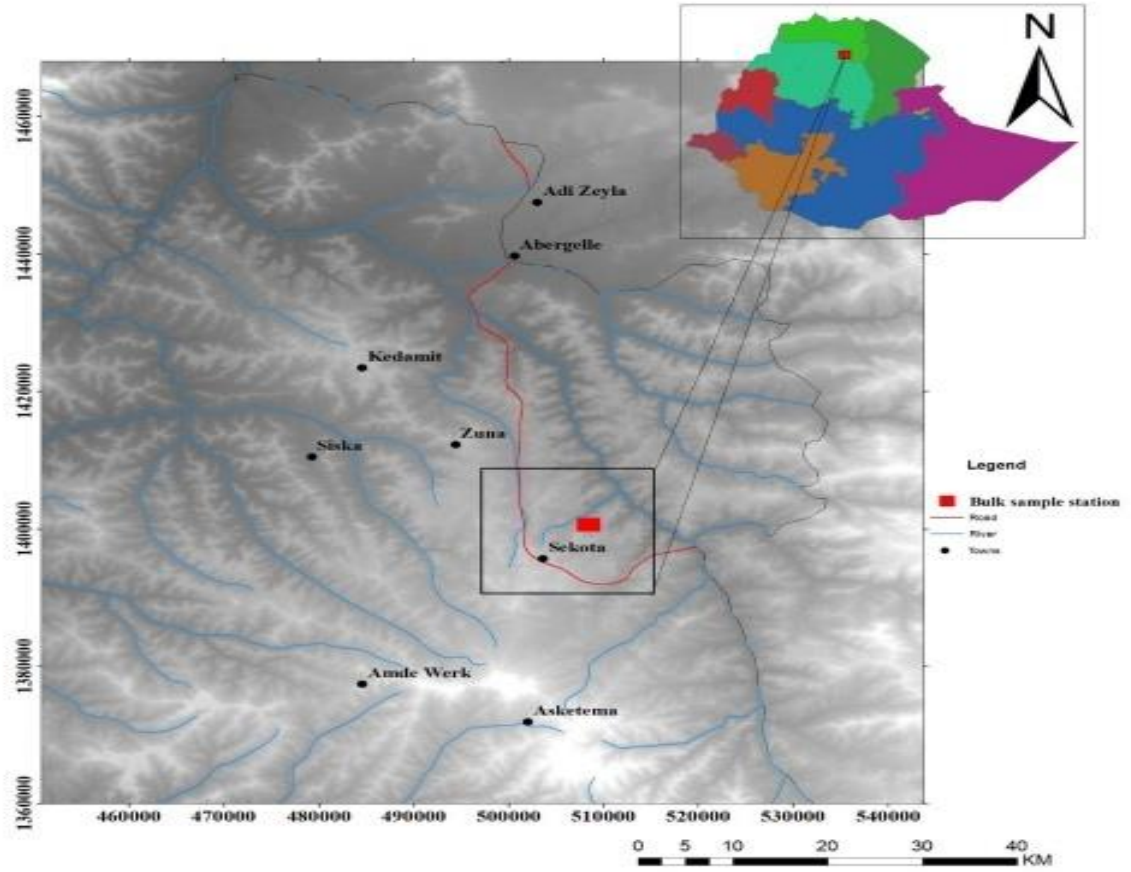

Figure 11. Location map of Akmayohanes hematite ore deposit, in Sekota woreda

3.2 Iron ore analysis methods

In the study area, the mineralogical characterization was done in 2016 by Sekota Mining Private Company. The mineralogy of the iron ore deposit was studied using an ore microscope (OM), XRD, and XRF. According to OM and XRD analyses, Sekota iron ore is mostly constituted of hematite, with minor goethite. The main impurities in this ore are silica and alumina, resulting in poor grade ore deposits. The ore microscope also revealed the texture of the ore minerals, as well as the hematite's liberability from the accompanying silicate matrix. The liberation size of Sekota iron ore ranges between 75 and 50 µm, indicating that fine grinding is required. XRF analysis was also used to identify the principal chemical components that were present in the iron ore deposits. Therefore, only physical grinding characterization of the bulk Sekota iron ore sample was performed based on the ball mill speed and milling time variation with respect to grindibility

and breakage properties of the iron ore, and the grinding characteristics of the iron ore was investigated by using laboratory ball mil (150×150mm) batch grinding test for three iron ore feed size fractions (-0.35+0.71mm,-0.71+0.15mm and -3.35mm) with varying mill fractional speed and grinding time.

3.3 Experimental work

Using a roll ball mill, batch milling experiments was carried out at the University of Addis Ababa Institute of Technology's Mechanical Unit Operation laboratory at the School of Chemical and Bioengineering. The experimental investigation of iron ore grindibility and breakage characteristics was carried out using samples prepared using a combination of crushing, sieving, and grinding, as shown in (Figure12). Apparatuses that are used for preparation of laboratory sample are: hammer, jaw crusher, ball mill, sieve, sieve shaker.

The effects of rotational speed, feed size distribution, and milling time on the grinding characteristics of Sekota bulk iron ore were assessed at five different mill fractional speeds, namely 250 rpm (7.1%), 300 rpm (8.6%), 350 rpm (10%), 450 rpm (12.8%), and 550 rpm (15.7%), as well as at six different milling times (5 min, 15 min, 25 min, 35 min, 45 min, and 60 min). Following are the feed sample size intervals that were taken into account for the test work: -0.710 +0.150 mm, -3.35 +0.71 mm and -3.35 mm. For each feed size interval, 318 gram was produced and processed in the laboratory ball mill. The mill speed is set at 450 rpm or 12.8% fractional speed for the milling time test, and the mill speed test was done at 25 minutes for each fractional speeds. The product size distribution analysis was carried out at the end of each milling test.

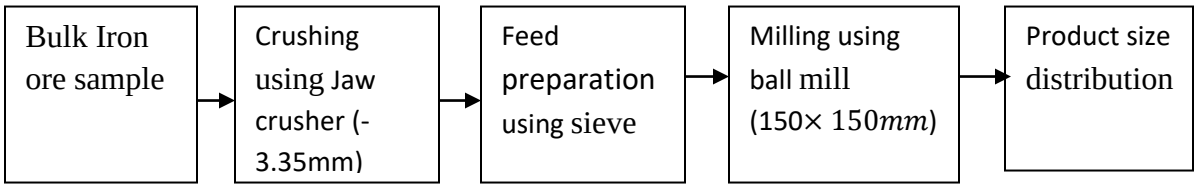

Figure 12. Shows a general experimental work flow diagram for an iron ore sample.

4. Geology and Mineralogy of Sekota Iron Ore

4.1 Geological Setting

4.1.1 Regional geology

Sekota and its surroundings are geologically located among the rock assemblages of the northern Ethiopian rock shields. The northern Ethiopian rock assemblage consists of complex rocks ranging in age from the Precambrian in the deep dissected zone to recent Mesozoic sedimentary rocks and Tertiary volcanic rocks. Precambrian rocks are metamorphosed meta-volcano sedimentary rocks. This is made up of clastic deposits, greywacke, basic Meta volcanic, phyllite, slate, and marble with prominent quartz veins and vein lets. The Precambrian rocks are well exposed in the dissected zone of the Tekeze river basin and appear to continue northwards to central Tigray. According to Stern (1994), these rocks are thought to have developed during the Precambrian period, during the East African orogeny. The Precambrian rocks are layered with thick Mesozoic sediments and tertiary volcanic (SMP, 2016).

Mesozoic rocks are made up of continental and marine deposits that developed between the late Paleozoic and early Mesozoic eras. These Mesozoic sediments are varyingly covered by Tertiary volcanics that erupted at the start of the Eocene. Tertiary volcanic features include a thick outpouring of fissuring flooded basalt forming flow, cones, and plugs, followed by the eruption of alkaline basalts and trachyte, as well as the pre-existing structures. The Sekota region is a transition zone between Tertiary volcanic rocks of the central Ethiopian highlands and Mesozoic rocks. In the Sekota region, this transitional nature promotes some commercial minerals such as hematite (iron ore), dimension stones, zeolites, and gemstones (SMP, 2016).

4.1.2 Local geology

According to SMP (2016), Sekota iron ore deposit is coved with sandstone, clay, mudstone and basalt. Based on their age, textural and mineralogical properties, the rock types that are found in the project area are classified as; ferruginized basalt, upper sandstone, pinkish sandstone, brown sandstone, hematite bearing mudstone and basaltic flows. The description of each rock types is shown below.

Ferruginized Clay

This rock type has a dark to very dark brown hue, is fine grained, and is quite strong. This ferruginezid basalt is not found everywhere, but it is found around the intersection of Mesozoic deposits and basaltic dykes. It appears in the form of boulders and fragments on the top of pinkish sandstone (SMP, 2016).

Upper Sandstone

The upper sandstone formation, which comprises the majority of the Sekota iron ore deposit, has varied colors and contains many types of sandstone units with varying grain sizes(SMP, 2016).

Pinkish Sandstone

It is light grey to grey in color with pinkish dots on the surface, and its name is derived from the pinkish patches. This sandstone is fine to medium grained in most cases and reaches up to 3 m in thickness where weathering is less significant. It is underlain by hematite containing mudstone (SMP, 2016).

Brown Sandstone

Brown sandstone, also known as upper sandstone, is the main unit in the deposit area. It is light grey brownish grey in color, generally deep bedded, and fine-medium-coarse grained. It is usually found above the lower sandstone and below the thick Tertiary volcanic. This top sandstone unit is crossed by basic dykes that run south-west and are roughly 2 m thick on average(SMP, 2016).

Hematite bearing Mudstone

Hematite bearing sandstone is dark brown to brown fine to medium grained, when it is weathered it becomes more pinkish red and have conglomeratic and kindly shaped nature and at place it contains free pebble size silica. This unit is underlined by barren brown sand stone and overlying by pink sandstone. There are three hematite layers in the deposit. The first layer is dark brown in color and has conglomeratic nature. It has an average thickness of 4.5 m and occurs between pinkish sandstone and brown sand stone. The second hematite layer is similar to the first layer but it has low iron content with 2.5m thickness.

The third layer is pinkish grey in color and has an average thickness of 3 m, with low iron content as compared to the first and second hematite layers (SMP, 2016).

Basaltic flows

. Basaltic rocks also dominate the area, generating undulating hills and highly elevated mountain ranges. This formation is made up of two different types of rock units: scoriaceous and aphanitic basalts. Aphanitic basalt is younger than scoriaceous basalt. Basalt is often black to dark grey in color, with fine grained texture and columnar jointing (SMP, 2016).

4.2 Mineralogical Assessment on Sekota Iron Ore

4.2.1 Mineralogical Study

A comprehensive mineralogical investigation was carried out using two methods: optical microscope (OM) and X-Ray Diffraction (XRD). For a given iron ore sample, an optical microscope study was performed to collect information such as mineral phase study, mineral area wise distribution, grain size distribution, mineral liberation study, textural and structural studies, and photomicrography, whereas XRD was performed for major and trace mineral qualitative and quantitative analysis(SMP, 2016).

I. Optical Microscope Observation:

Mineral composition, microstructures, textures, and the interaction of valuable and gangue minerals are all revealed through ore microscope research. Overall, the studied sample is characterized by being significantly altered, as a result of which associations of toxic gangue minerals with other ore minerals have been discovered in significant amounts. The study revealed a low to moderate concentration of iron ore minerals (hematite and goethite) with a significant proportion of gangue minerals such as quartz and clay. According to detailed ore mineralogical analyses, an iron ore sample has 60% ore (hematite and goethite) and 40% gangue (ferruginous clay, quartz, and iron coated oxide) minerals by area of distribution (SMP, 2016). The ore and gangue minerals are described in detail below.

a) Hematite

The main and most abundant ore mineral, hematite contributes significant amounts, followed by goethite, which contributes somewhat more. Hematite is an ore mineral that makes up 40% of the area overall and can be found as huge, irregular masses or small, discrete mineral grains. Hematite with coarse grains is found with ferruginous clay and iron coated oxide as gangue minerals. Hematite occurs nearby with a small number of extremely tiny goethite grains and irregularly shaped masses, demonstrating how the grain boundaries have been altered. The minerals in this ore, which range in size from coarse to fine, may be thought of as an admixture. 180 microns to a minimum of 5 microns is the size range of hematite grains. Coarse grains are those that range in size from 180 microns to 100 microns and make up around 5% of the 40% hematite grains. The remaining 55% of grains are classified as fine grain and are found below the size of 30 microns. About 40% of grains are classified as medium grain and range in size from 100 to 30 microns (SMP, 2016).

Among the coarse grains, around 10% grains are in fully liberated state, whereas remaining 90% grains are in un-liberated state. These un- liberated grains are in association with the other grains at less than 90 micron size. Among the medium sized grains, around 28% grains are fully liberated state whereas remaining 72% grains are in un-liberated state. Among the small size grains, around 40% grains are in fully liberated state and the remaining 60% grains are in un-liberated state (SMP, 2016).

b) Goethite

Goethite is a secondary ore mineral occurring in the analyzed sample. The iron ore which contains goethite as secondary ore mineral do contribute some amount of moisture. In the investigated sample, goethite occurs in approximately 20%area by its area distribution. This ore mineral accommodates some gangue mineral association around its margin i.e. ferruginous clay. Maximum grain size of goethite grain is around 150 micron size. Around 20% area is covered with coarse sized grains which are in 150 to 100 micron size, while around 50% area coved with medium size grains which are in 100 to 30 micron size. The remaining 30% area is covered by small size grains which are in less than 30 micron (SMP, 2016).

Among the coarse grains, around 10% grains are in liberated state whereas the remaining 90% grains are in un-liberated state. These un-liberated grains show close association with other ores and gangue minerals at less than 100 micron size. Among the medium size grains, around 22% grains are in liberated state whereas the remaining 78% grains are in un-liberated form. These un-liberated grains show close association with other ore as well as gangue minerals at less than 60 micron size. Among the fine sized grains, around 30% grains are in liberated form while the remaining 70% grains are in un-liberated state (SMP, 2016).

c) Quartz

Quartz is the major gangue mineral present in Sekota iron ore sample and that covers 20% of the total area. Texturally, quartz grains are classified as large, medium and small sized grains. Coarse sized grains are in 130 to100 micron size, medium grains are in 100 to 30micron size and small sized grains are in less than 30 micron size.

Among the quartz grains, coarse sized grains cover 15% of the area and from which around 30% grains are in liberated form while 70 % grains are un-liberated. These un-liberated grains show close association with the other ore and gangue minerals grains at less than 80 micron size. Medium sized grains cover around 35% of the total area, from which 35% of grains are in liberated state while the remaining 65% grains are in un-liberated state. These un-liberated grains show close association with the other ore as well as gangue minerals at less than 60 micron size. Fine sized grains also cover 50% as a whole, from which around 45% grains are in liberated state whereas the remaining 55% grains are in un-liberated state. These un-liberated grains show close association with other ore as well as gangue minerals at less than 20 micron size (SMP, 2016).

d) Ferruginous clay

It is also a major gangue mineral next to quartz in the analyzed sample and occurs at ground mass and at the margin of few ore and gangue minerals in several places. It occurs around 18% of area as whole. This gangue occurs as irregular shape and very fine size, argillaceous minerals which may contains some clay minerals. Due to very fine size and submicroscopic in nature these grains (<5 micron) are occurred as patches and cannot identified through optical microscope. The maximum size of the patch is 200 micron.

e) Iron coated oxide

This gangue mineral is also termed as pseudo ore; it is next to quartz in abundances. As a whole this gangue mineral occur as very fine grain interstitial mineral matter which most of the ore minerals at less than30 micron in size, and it covers total area around 2% as a whole and none of this grains are in liberated stat(SMP, 2016)e.

II. XRD analysis

To obtain detailed information about the major and trace minerals phases present in the analyzed sample, XRD analysis was used and the analysis result showed that the Sekota iron ore is composed of hematite (45%) and goethite (15%), quartz (27%), kaolinite (11%) and minor phase illemanite (2%)(SMP, 2016).

4.2.2 Mineral Liberation Study

Gangues mineral inter- locking with valuable mineral liberation are interdependent factors and are very critical in analyzed iron ore sample. The silicate gangues inter- locking with the hematite ore do not show clear trend. Major ore mineral is hematite covering approximately 40% of the total area, followed by goethite with 20% area. The liberation size of hematite and goethite is ranging from 75 to50 µm. however, large amount of goethite particles are in un- liberated state and thus, it is considered to be a gangue mineral like quartz and clay (SMP, 2016).

As a whole, out of 40% hematite, around 13% grains are fully liberated state and remaining 27% are in un-liberated state. These free hematite ore particles are found between 180 and 30µm and from which less than 4% free iron ore particles are in the range of 180 to 30µm while the remaining 9% grains are at less than 30 µm. from the total 27% un-liberated grains, around 14% grains are found in the range of 180 and 30 µm and could be liberated around 50 µm, and the remaining 13% un- liberated grains are in less than 20 micron size. Among goethite grains which cover 20% of total area, around 4% grains are in free- state and the remaining 16% grains are in un-liberated state. Among the total free-state grains, around 2% grains are in 150 to 30µm and the remaining 2% free grains are in less than 30 micron size. From 16% un-liberated iron ore particles, around 12% grains are in 150 to 30 micron size. Remaining 4% un- liberated grains are less than 30 micron size. The un-liberated grains are associated with grains of quartz and clay minerals (SMP, 2016).

Quartz grains are distributed at around 20% area as a whole, out of which around 8% grains are in free- state while the remaining 12% grains are in un-liberated state. Among the free quartz grains, around 4% grains are in 130 to 30 micron size and remaining 4% grains are in less than 30 micron size. Among un- liberated grains 7% grains are in 130 to 30micron size and could be liberated at around 60micron size. The remaining 5 % grains are in less than 20 micron size (SMP, 2016).

Other gangue mineral present in analyzed sample are ferruginous clay and iron oxide coated clay gangue ferruginous clay is amalgamation of submicroscopic size mineral grains which occurs in patches of at margins of ore and gangue minerals and at ground mass as well. None of ferruginous clay is free- state. Iron oxide gangue also termed as pseudo ore which covers 2% of total area. All grains of this mineral are less than 30 micron size and none of these grains are in free- state (SMP, 2016).

Ore/ Gangue Mineral	Overall Dist. Area wise (%)	Grain Size µ		Area Covers (%)	%, Dist. (Wrt OM)	Fully Lib. Grains (%)	Lib. Grains (%) (Wrt OM)	Un-lib. grains (%)	%, Dist. Unlib. Grains (Wrt OM)	Unlib. Gangue size(µ)
Hematite (H)	40	Coa	180-100 µ	5	2	10	0.20	90	1.80	< 90 µ
		Med	100-30 µ	40	16.0	28	4.5	72	11.5	< 50 µ
		Sma	< 30 µ	55	22.0	40	8.8	60	13.2	< 20 µ
							13.5		**26.5**	
Goethite (G)	20	Coa	150-100 µ	20	4	10	0.4	90	3.6	< 100
		Med	100-30 µ	50	10	22	2.2	78	7.8	< 60
		Sma	<30µ	30	6	30	1.8	70	4.2	< 20
							4.4		**15.6**	
Quartz (Q)	20	Coa	130-100 µ	15	3	30	0.9	70	2.1	< 80
		Med	100-30 µ	35	7	35	2.45	65	4.55	< 60
		Sma	<30µ	50	10	45	4.5	55	5.5	< 20
							7.9		**12.2**	
Ferruginous Clay (FCL)	18	Coa Med Sma	<200µ	100	18.0	Nil	Submicroscopic size grains occurs as patches of irregular shape and sizes			
Iron Oxide Coated Gangue (IOCG)	2	Coa Med Sma	<30µ	100	2.00	Nil	All pseudo Ores grains are masked by other ore and gangue minerals.			

Table 9: Shows detail liberation properties of valuable and gangue minerals of Sekota iron ore deposit (SMP, 2016).

5. Result and Discussion

5.1 General

For a certain feed ore material, a number of factors affect the grinding process. These include the size, shape, and type of the grinding media, the volume of the feed and the ball charge, the mill speed or critical speed, the milling time, the concentration of the slurry during wet milling, the distribution of the feed size, and the characteristics of the feed material i.e. hardness and brittleness (Gupta and Sharma, 2014 &Austin et al., 1984). To investigate the grinding properties of a bulk sample of iron ore material obtained from the Sekota iron ore deposit in the Akmayohanes location, the research was used the mill rotational speed, feed size distribution, and milling time.

5.1.1 Effect of mill speed on ball mill performance of iron ore

In this study, the effect of mill speed on ball mill performance iron ore is evaluated based on its power consumption, desired grind size and product size distribution. The effect of mill speed on the performance of the ball mill is evaluated using three distinct iron ore feed size fractions (-3.35+0.71mm,-0.71+0.15mm and-3.35mm) with five different mill speed (250 rpm, 300 rpm, 350, rpm, 450rpm and 550 rpm).

I. Effect of mill rotational speed on grind size and P80

Mill speed is one of the key elements influencing the intended grind size. The mass fraction passing 0.075mm is ideal for assessing grind size (Levin, 1992). This investigation was found to be even more important since the Sekota iron ore requires finer grinding to liberate the iron element from silica and alumina impurities. The quantity of desired grind size, which is -75µm, is increased until the maximum mill speed is attained. The highest mill speed is 450 rpm, and at this speed, the cumulative percent passing of 75µm for feed sizes: -3.35+0.71mm, -0.71+0.15mm, and -3.35mm is 27%, 36%, and 49.4% respectively. The intended quantity of grind size, higher than or equal to 75%, is not obtained by this speed in the three feed size fractions, although the mixed feed size fraction produces more grind size (49.4%) than the other two size fractions (Figure13).details of the grind size and P80 values for each size fractions of iron ore feed with the corresponding mill rotational speeds is shown in (Table10).

Feed size(mm)	Speed(rpm)	Cum.wt.% passing of 0.075mm	P80(µm)
0.355+0.71	250	7.5	1875
	300	10.3	1846
	350	19.1	1014
	450	27.0	448
	550	11.2	1329
-0.71+0.15	250	10.7	309
	300	14.9	357
	350	30	161
	450	36.4	151
	550	15.3	328
-0.355	250	15.5	1988
	300	16.5	1817
	350	29.7	226
	450	49.4	204
	550	14.9	666

Table 10: Result of cum.weight % passing of 75µm and P80 for each feed size fraction with different mill rotational speed.

Mill rotational speed also affects the product size distribution of different iron ore feed size fractions. As shown in the product size distribution curve of each feed size fractions, the cumulative weight % passing of 80 % of the feed iron ore particles (P80) is generally decreased until maximum mill fractional speed (12.8%) is attained. At maximum mill speed (450 rpm), the P80 value of the feed size fraction of -335+0.71mm,-0.71mm and -0.35 mm are 448 µm, 151 µm and 226 µm respectively. The P80 value of -0.71+0.15 mm feed size fraction is low as compared to the other two feed size fractions because 12.8% is considered to be low speed and at low speed milling, fine feed size particles are easy to grind than coarse feed size particles. As illustrated in (Figure14) and product particle size curves (Figure 15,16&17), 450 rpm and 350 rpm provide low P80 values in all iron ore feed size fractions when compared to mill rotational speeds of 250 rpm, 300 rpm, and 550 rpm.

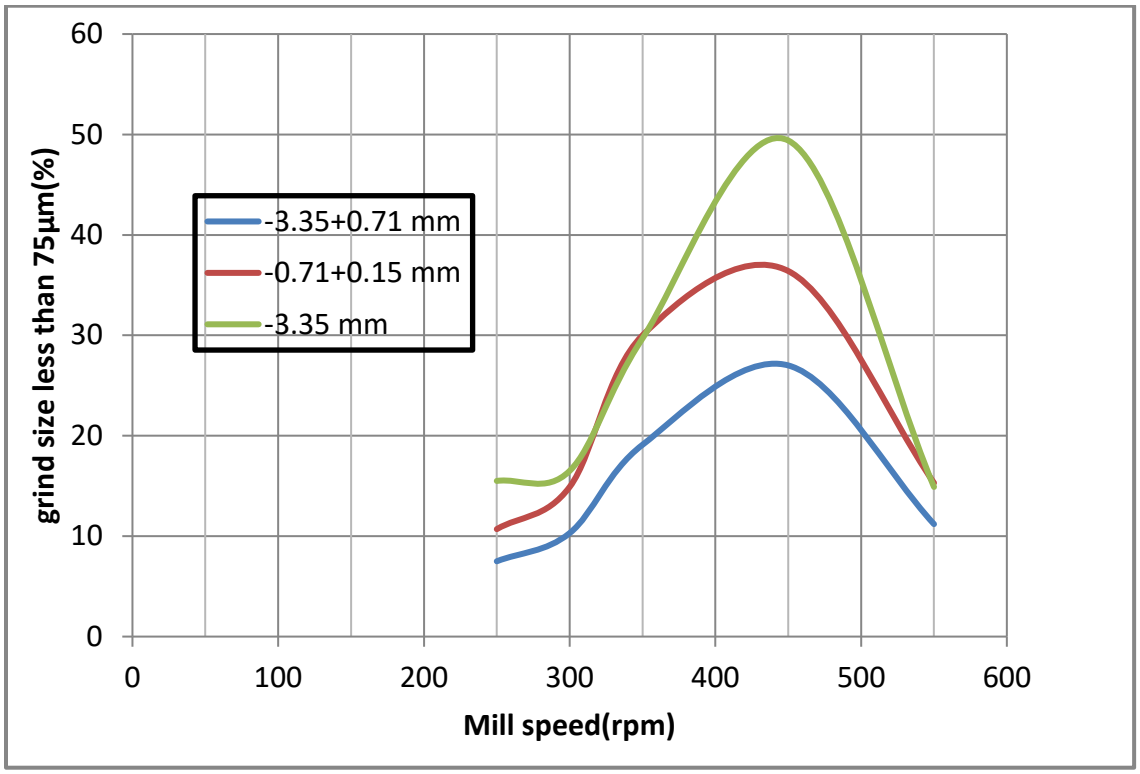

Figure 13: Effect of mill speed on the grind size of different iron ore feed size fractions.

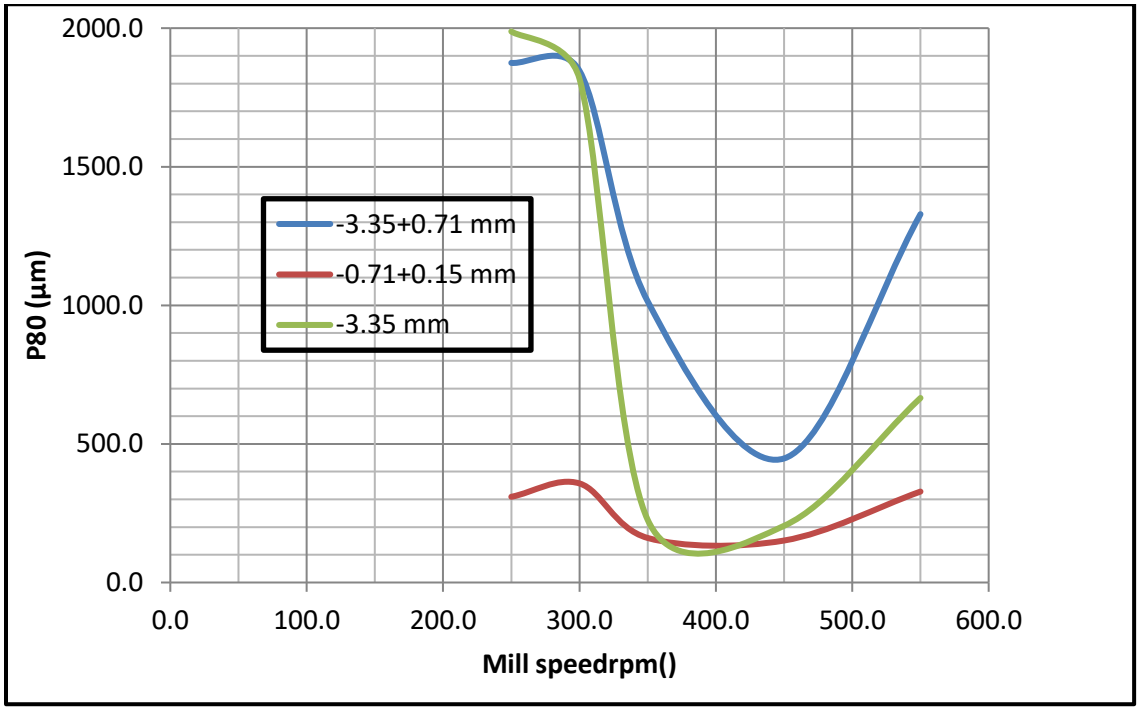

Figure 14: Effect of mill speed on the P80 of different iron ore feed size fractions.

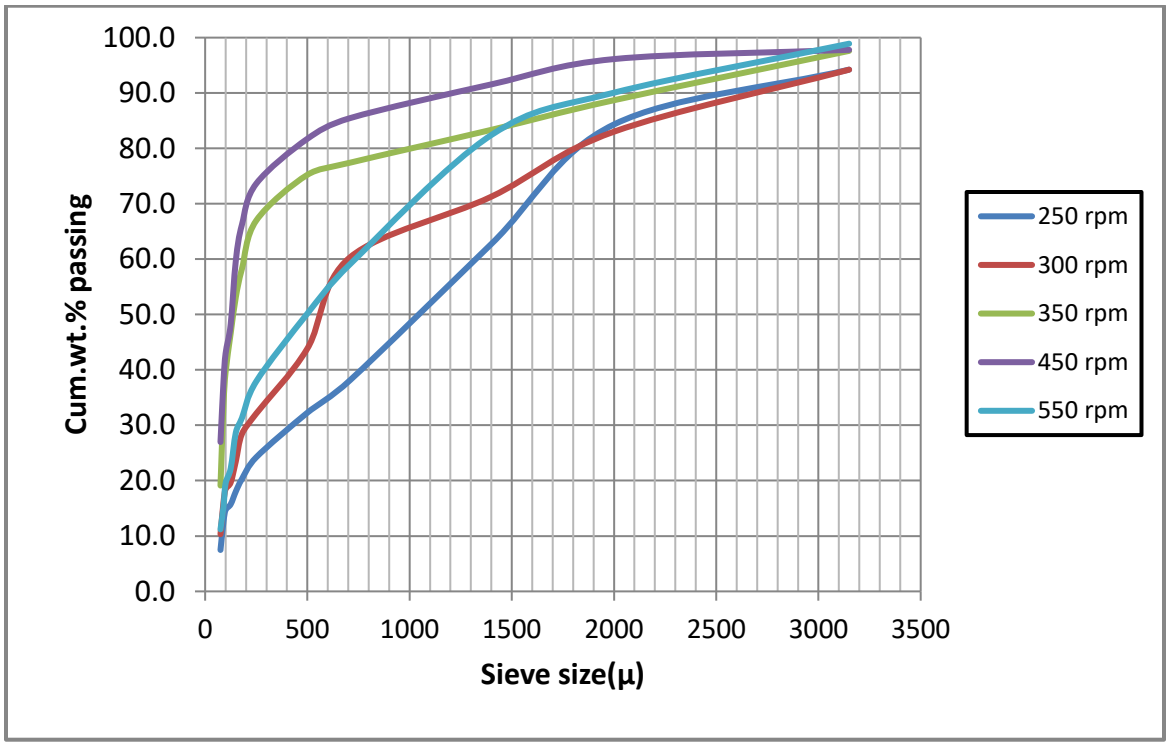

Figure 15: Product size distribution analysis for -3.35+0.71 mm iron ore feed size fractions.

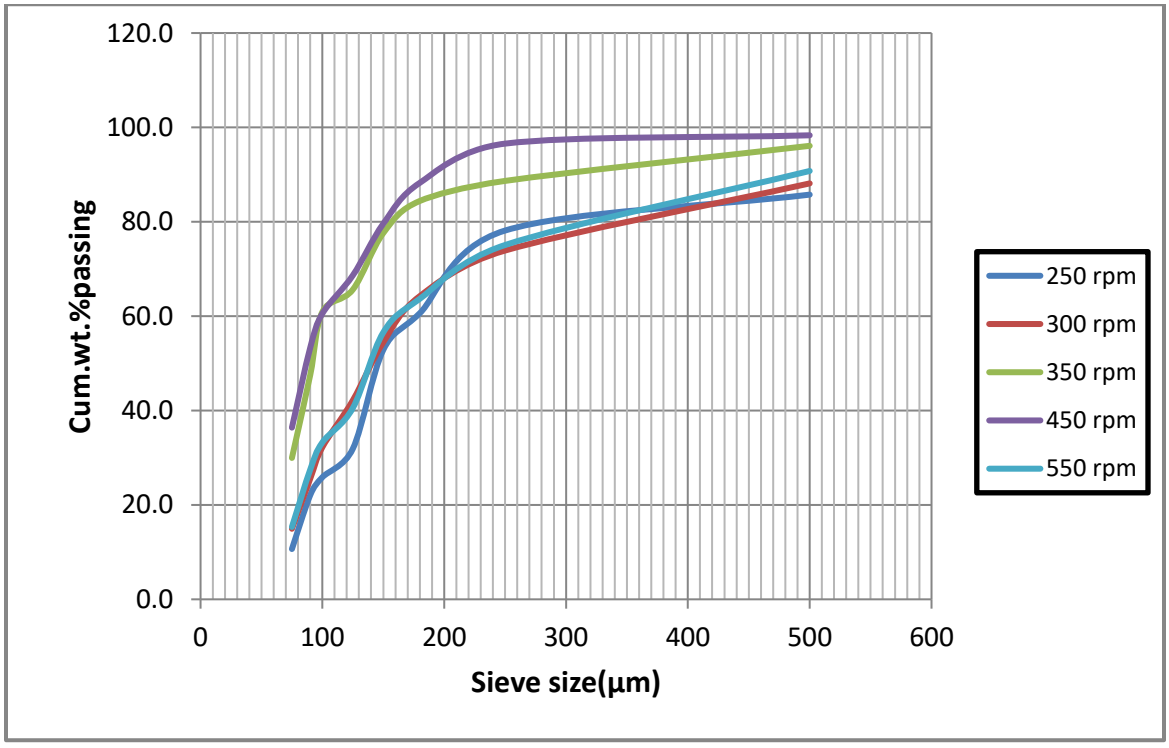

Figure 16: Product size distribution analysis for -0.71+0.15 mm iron ore feed size fractions

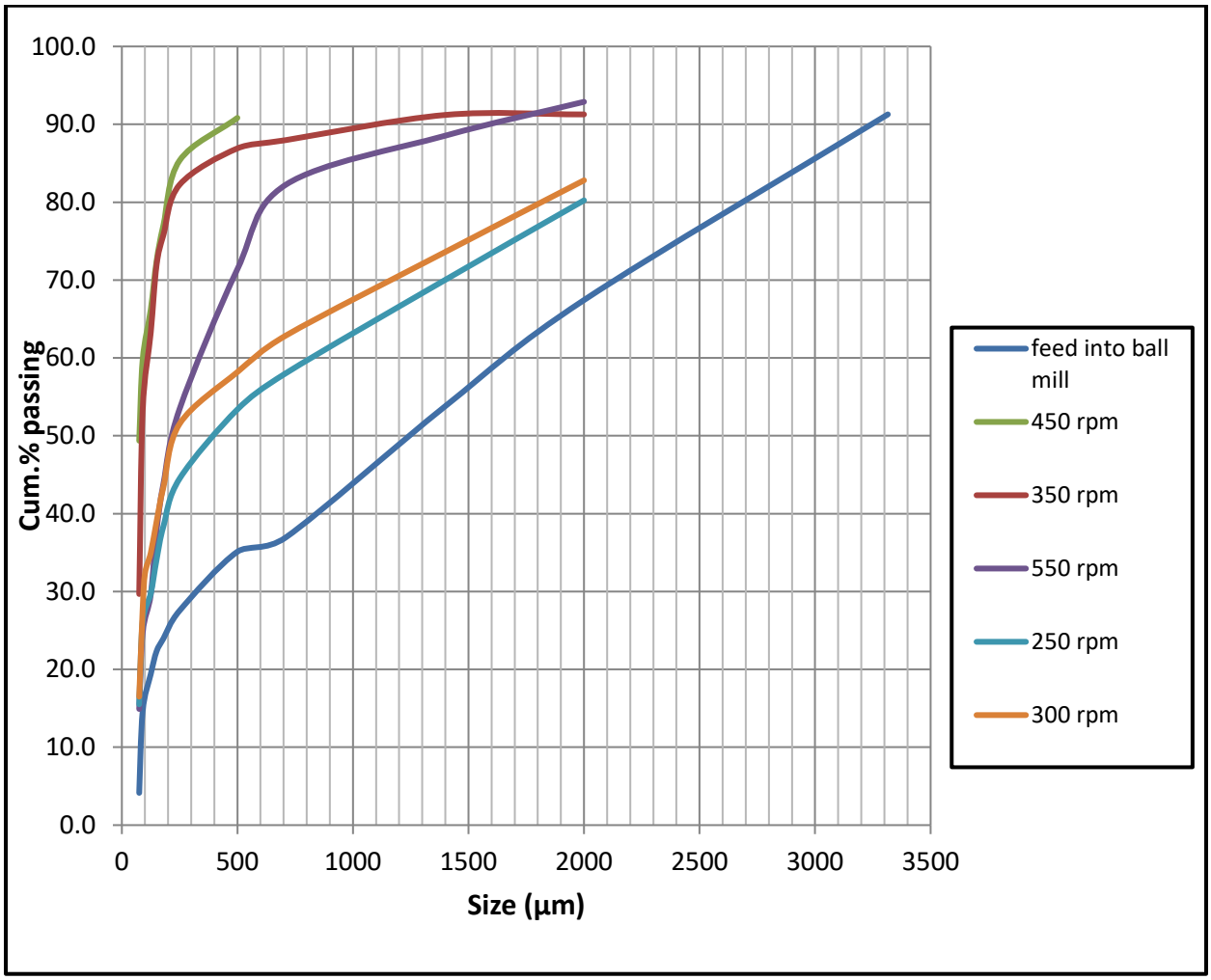

Figure 17: Feed and product size distribution analysis for -3.35mm iron ore feed size fractions

II. Effect of mill rotational speed on power drawn

The power draw is defined as the rate at which potential and kinetic energy are transmitted to the charge in the mill. Increasing the mill speed increases both the imparted kinetic energy and the potential energy As a result; larger power demands are projected as mill speed increases (Shi and Xie, 2015). Kelly and Spottiswood (1982) have shown in Figure18 that power increases with mill rotational speed only up to a point before power begins to diminish. As the speed increases, the material begins to centrifugal, resulting in a loss of power. The maximum power consumption was discovered to be approximately 90% of the critical speed (Figure18), and mineral processing industries typically run ball mills around 75%.

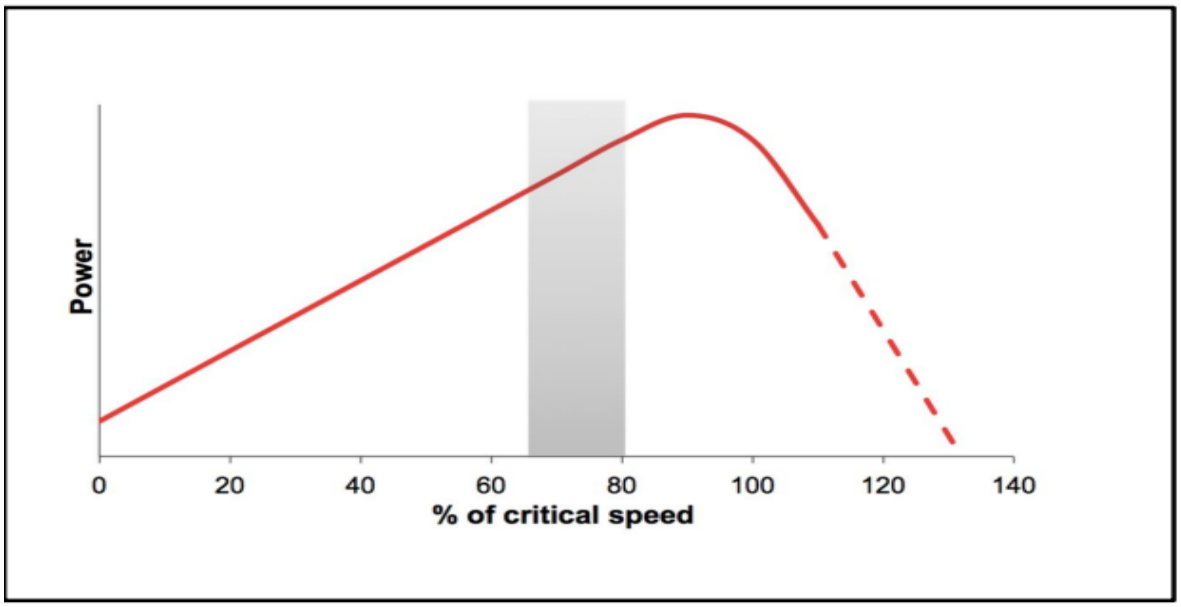

Figure 18: Variation of the power draw of a ball mill with its rotational speed (after Kelly and Spottiswood, 1982).

There are several approaches for determining mill power draw. In this investigation, the mill power is calculated based on Stamboliadis (2011) and Bond (1952) developed equation, and the equation parameters are listed in Table11 and Table 14 respectively.

$$Pnet = 9.9.\ M.\ N.D \quad \text{.....Equation (9)}$$

$$P_{B=}10wi\ [\frac{1}{\sqrt{P80}} - \frac{1}{\sqrt{F80}}] \quad \text{.....Equation (10)}$$

Table 11: Mill power calculations: the total load mass (i.e. mass of balls and sample) is M = 3.25+0.318 = 3.57kg; the rotational speeds are N= 0.12, 0.14,0.17,0.21 and 0.26 rps, equivalent to 7.1%(250rpm), 8.6%(300rpm),10%(350rpm) ,12.8%(450rpm) and 15.7%(550rpm) of the critical speed, respectively; and the mill diameter D=0.15m.

N_C (rps)	M(kg)	D(m)	P(W)
0.12	3.57	0.15	0.64
0.14	3.57	0.15	0.74
0.17	3.57	0.15	0.90
0.21	3.57	0.15	1.11
0.26	3.57	0.15	1.38

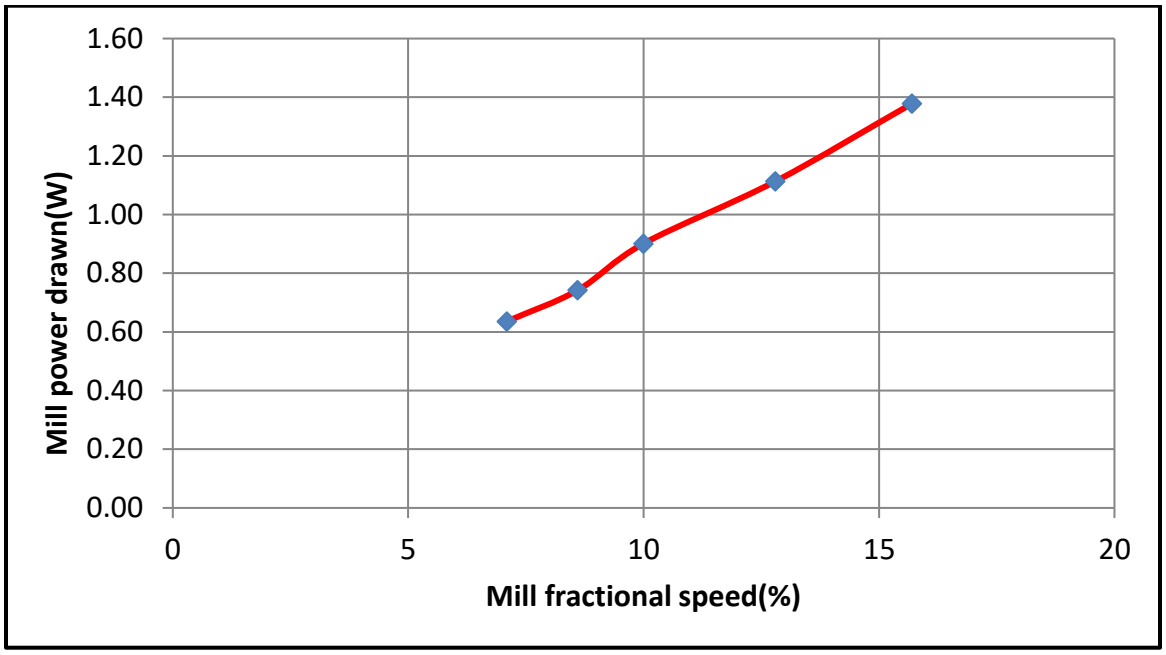

Figure 19: Shows variation of mill power draw with changing mill rotational speed.

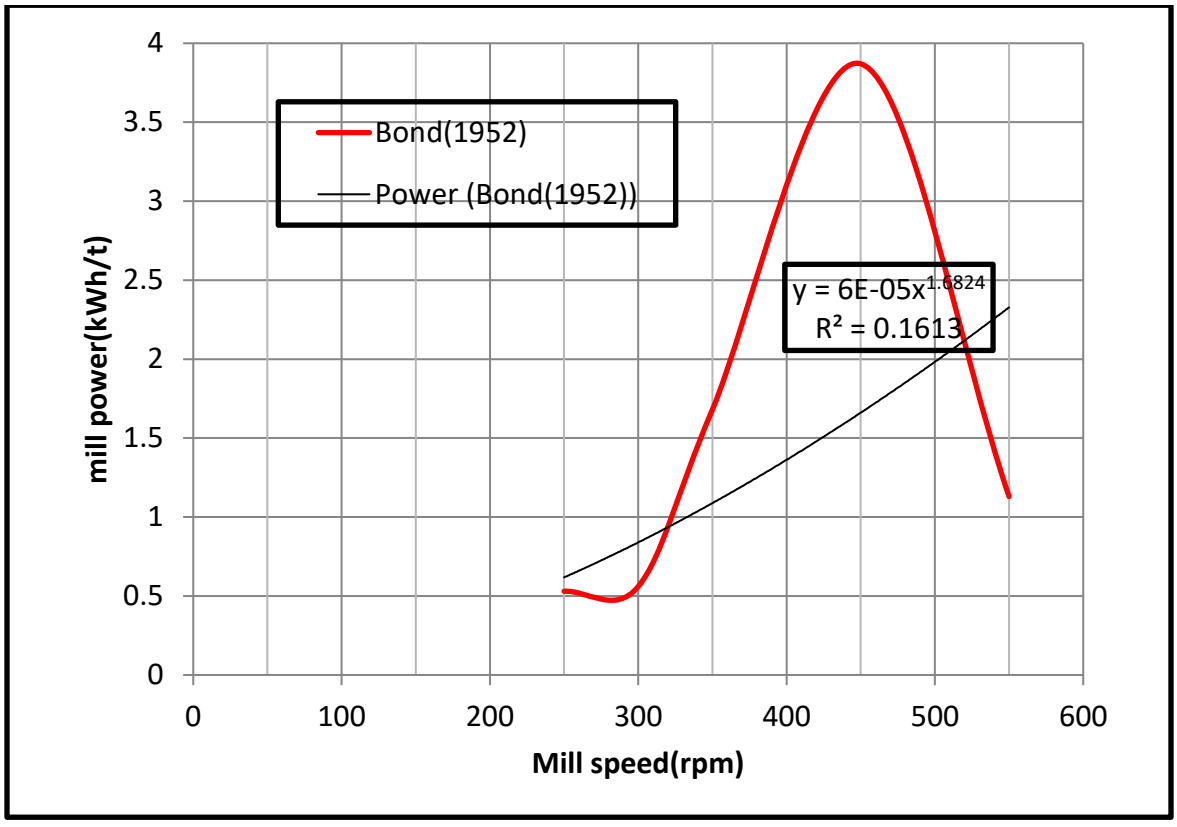

Figure 20: Effect of mill rotational speed on Bond's ball mill power during milling of -3.35mm iron ore feed size.

For -3.35mm feed size the effect of mill rotational speed on the Bond's ball mill power is determined and the mill power increased from 0.53 to 3.87 kWh/t when mill speed changing from 250 to 450 rpm and then decreased from 3.87 to 1.13 kWh/t when mill speed increased from 450 to 550.This indicated that mill speed and Bond's ball mill power do not have linear relationship rpm (Figure20).

5.1.2 Effect of milling time on grinding performance iron ore

The influence of milling time on ball mill grinding performance of iron ore is also evaluated in this study based on power consumption, intended grind size, and product size distribution. The influence of milling time on ball mill performance is investigated utilizing three distinct iron ore feed size fractions (-3.35+0.71mm,-0.71+0.15mm, and-3.35mm) and six different grinding times (5min, 15min, 25min, 35min, 45min, and 60 min).All iron ore feed size fractions are processed at 450 rpm (12.8%) which is the highest fractional speed of the laboratory ball mill.

A. Effect of milling time on grind size and P80

The mass percent of target grind size, which is -75µm, typically increases with increasing milling time, ranging from 8.5 to 31%, 7.1 to 22.8%, and 10.6 to 26% for coarse(-3.35+0.71mm), fine(0.71+0.15mm), and bulk(-3.35mm) iron ore feed size fractions, respectively. Long grinding times (25, 35, 45, and 60 minutes) provide more desirable grind size than short grinding times (5 and 15 minutes) with the same mill rotational speed (450 rpm). However, neither short nor long grinding processes produced the required quantity of grind size (>75%). More fines are formed in the coarse feed size fraction (0.355+0.71) at 35min, 45min, and 60min, but the fine feed size fraction (-0.71+0.15) is insignificantly impacted by extended grinding time at this rotational speed (Figure 21).Details of the grind size and P80 values for each size fractions of iron ore feed with the corresponding milling times is shown in (Table12).

Feed size(mm)	time(min)	Cum.wt.% passing of 0.075mm	P80(µm)
0.355+0.71	5	8.5	2185
	15	11.9	1786
	25	29.2	731
	35	30.1	184
	45	30.6	178
	60	31.1	184
-0.71+0.15	5	7.1	359
	15	8	221
	25	21.2	199
	35	21.9	176
	45	22.4	156
	60	22.8	147
-0.355	5	10.6	1870
	15	12.2	978
	25	20.2	413
	35	21.3	344
	45	22.8	218
	60	26	152

Table 12: Result of cum.weight % passing of 75µm and P80 for each feed size fraction with different milling time.

Milling time, like mill rotational speed, influences the product size distribution of various iron ore feed size fractions. As demonstrated in the product size distribution curves (Figure23, 24&25) and p80 versus time graph (Figure22) for each feed size fraction, the cumulative weight% passage of 80% of the product iron ore particles (P80) generally decreases from 5 to 60 minutes of grinding time. However, the P80 of -0.71+0.15 mm feed size fraction is remain constant at the longest grinding time. The P80 value of the feed size fraction of -335+0.71mm,-0.71mm, and -0.35mm at the longest grinding time (60min) is 184 m, 147 m, and 152 m, respectively. The P80 value of -0.71+0.15 mm feed size fraction is slightly lower than the other two feed size fractions because 12.8% is considered low speed milling and fine feed size

particles are relatively easier to grind than coarse feed size particles at low speed milling because fine feed size particles have a larger surface area than coarse feed size particles, resulting in better ball to ore particle contact.

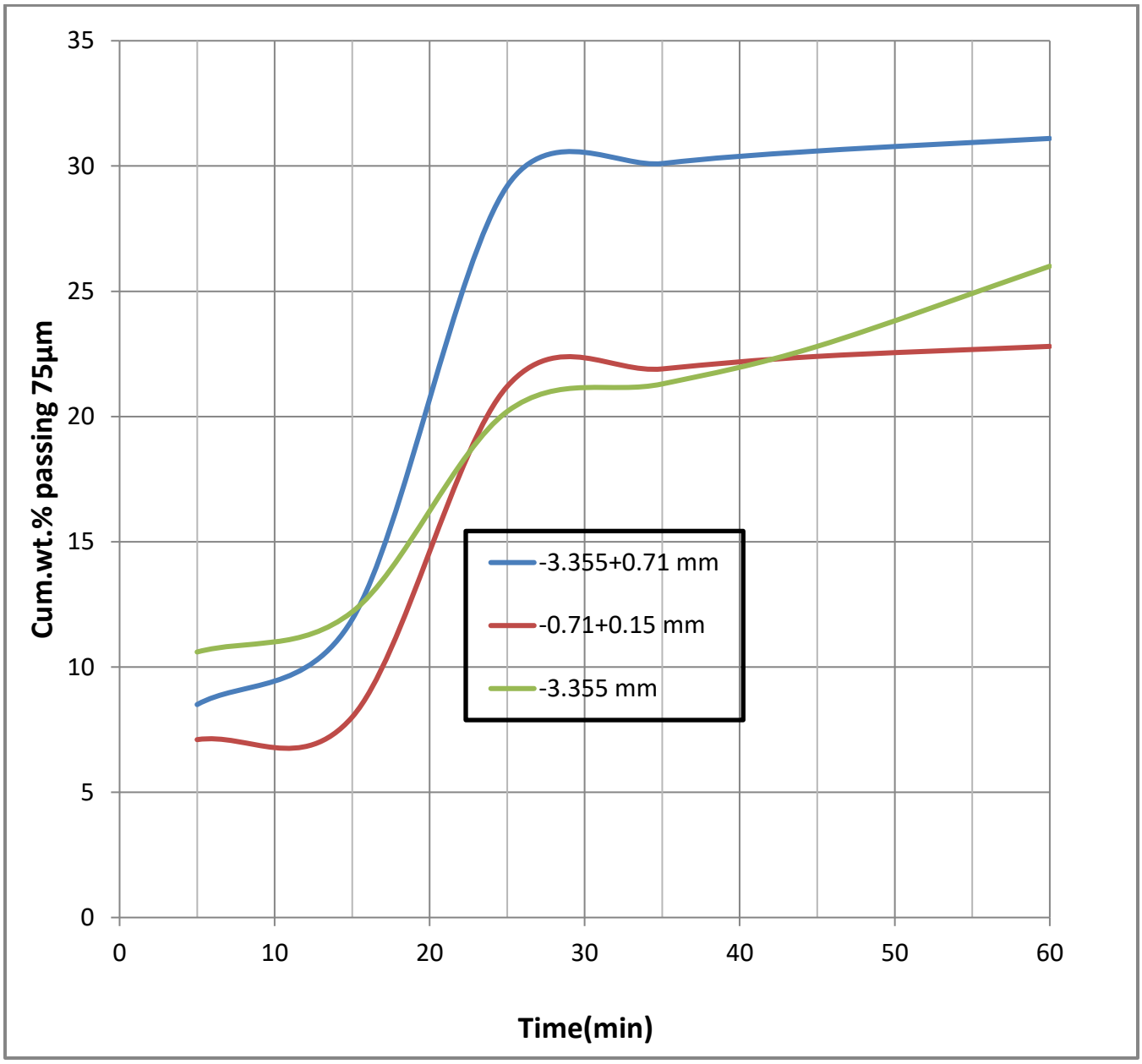

Figure 21: Effect of milling time on the grind size (-75µm) of different iron ore feed size fractions.

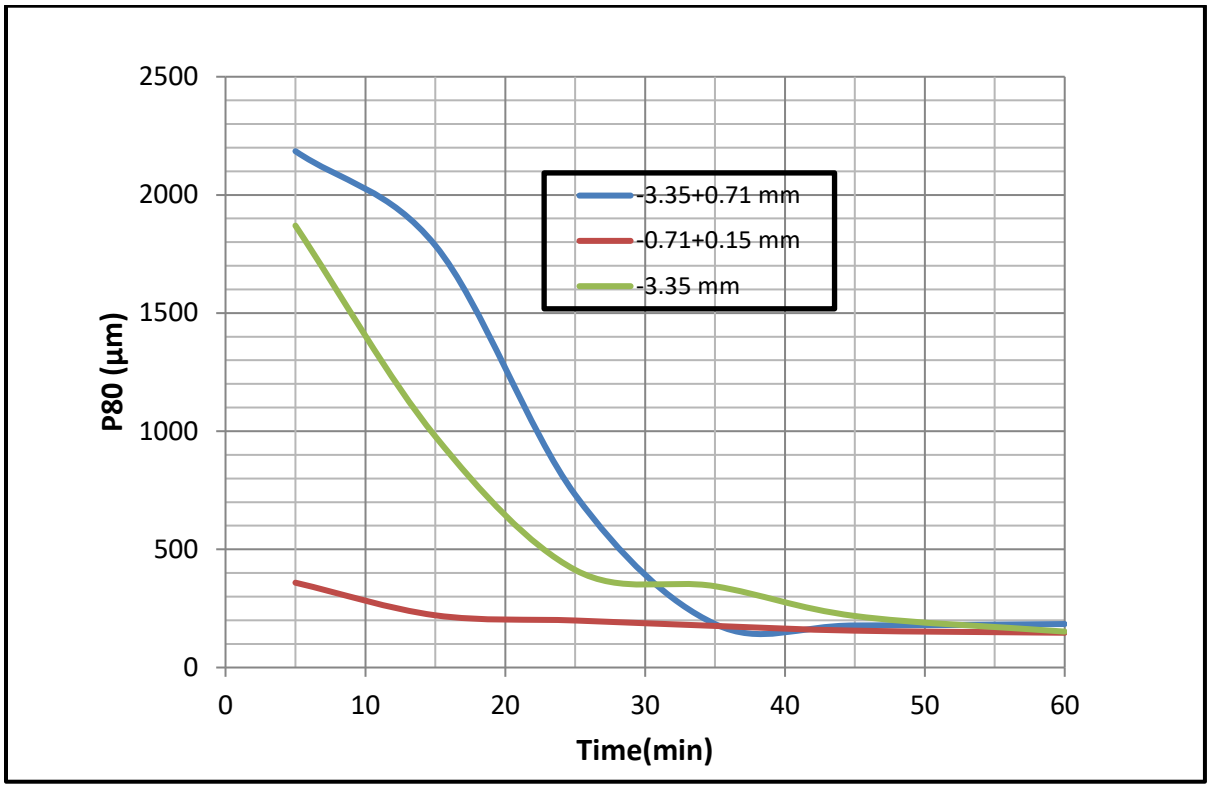

Figure 22: Effect of milling time on the P80 of different iron ore feed size fractions.

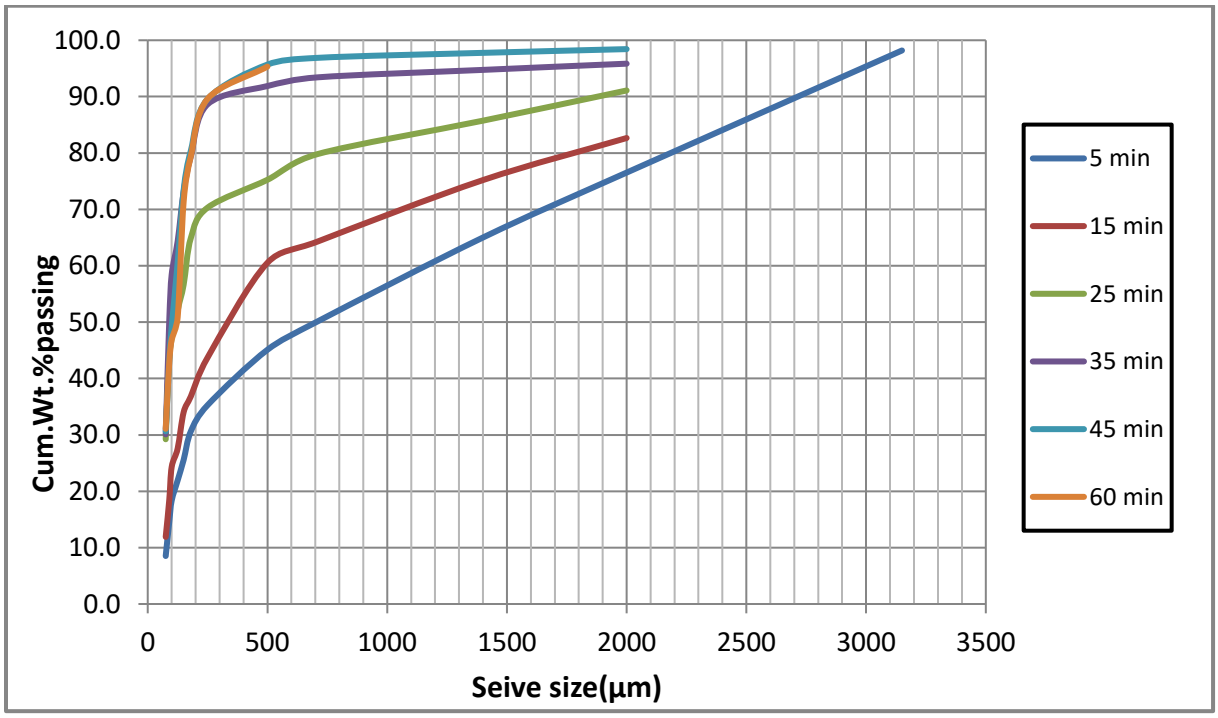

Figure 23: Product size distribution analysis for -3.35+0.71 mm iron ore feed size fractions with changing milling time.

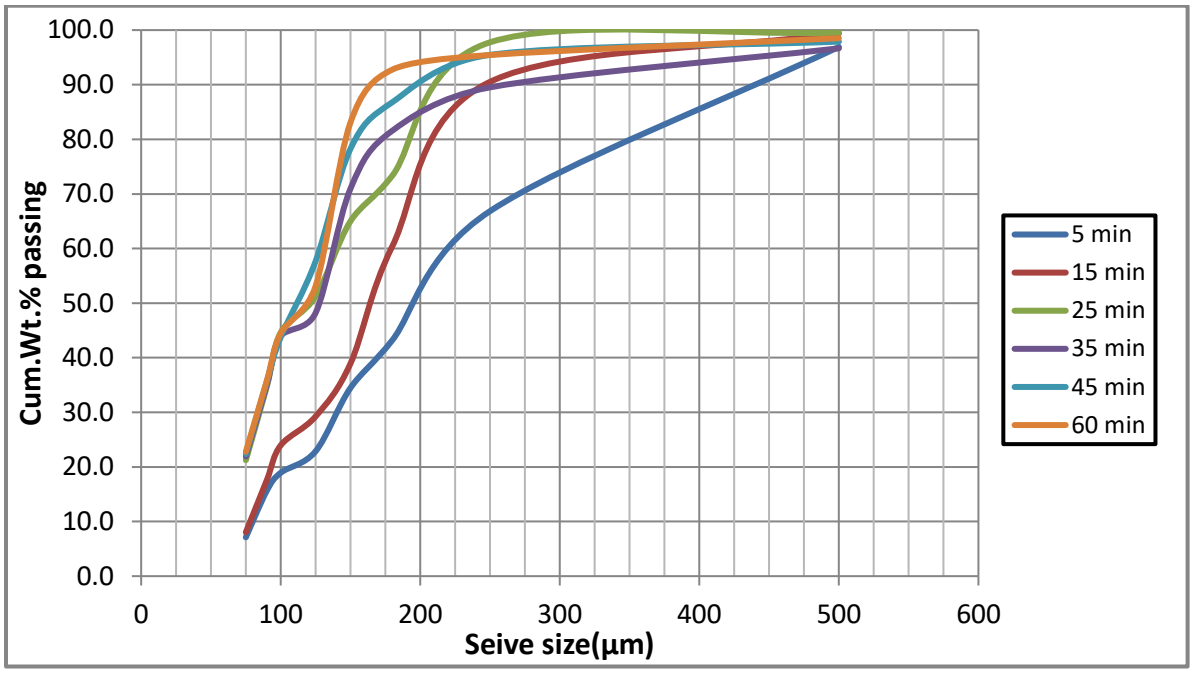

Figure 24: Product size distribution analysis for -0.71+0.15 mm iron ore feed size fractions with changing milling time.

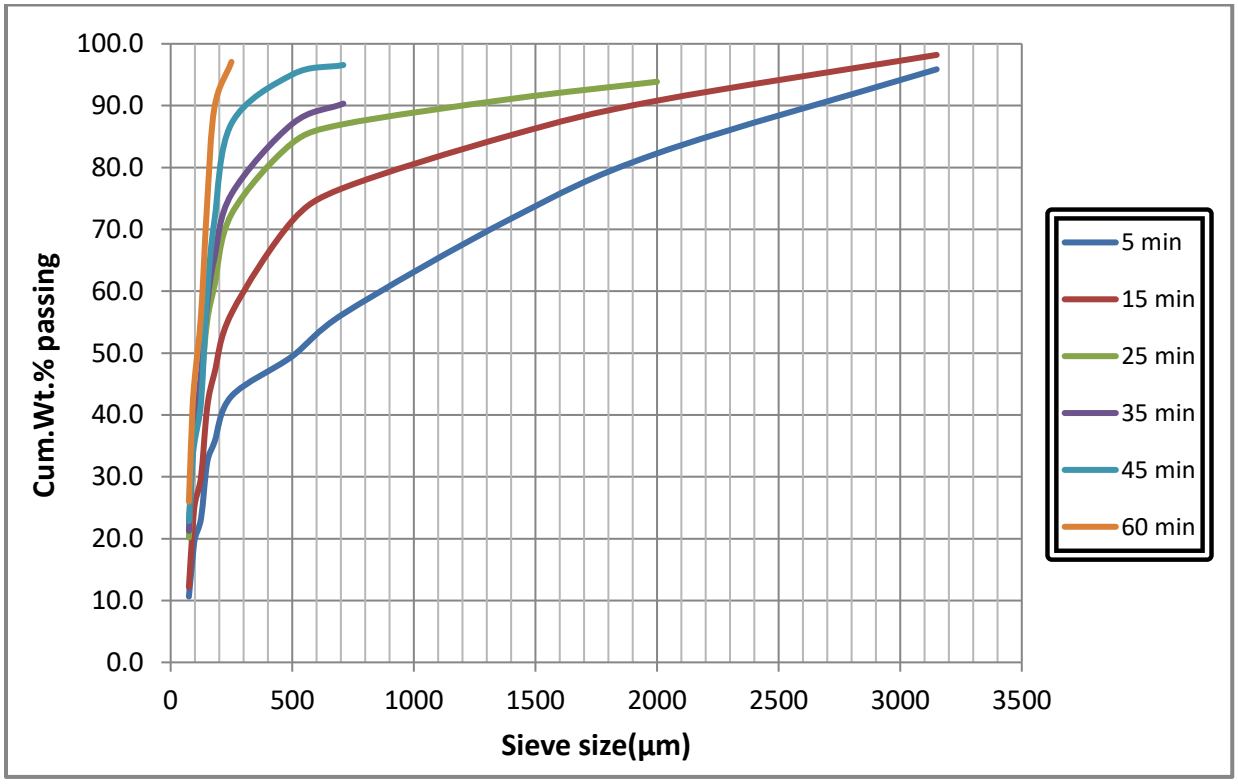

Figure 25: Product size distribution analysis for -0.335 mm iron ore feed size fractions with changing milling time.

B. Effect of milling time on power drawn

Milling time has a substantial influence on the power consumption of the ball mill when milling different iron ore feed size fractions (-3.35+0.71mm,-0.71+0.15mm and -0.355mm) at the maximum rotating speed of 450 rpm. The energy consumption of the three feed size fractions was determined using the equation (E=Pt), and the estimated values of the ball mill energy consumption for 5min,15min,25min,35,min,45 min and 60 min are presented on the (table13). As shown in the Figure 26, the energy consumption of ball mill is linearly increased from 5 to 60 min with fixed power (1.11W) and the consumed energy during grinding of iron ore is ranging from 5.55 to 66.6 joule.

To determine the Bond's (1952) mill power, 13.84kwh/t of hematite work index and 2700µm F80 of the bulk iron ore feed size were used. The work index of hematite is adopted from literature and the F80 of the iron ore was determined from feed size distribution curve.

Mill power increased from 0.54 to 8.55 kWh/t during milling of -3.35 mm feed size. The relationship is linear and different from the relationship between mill speed and mill output. This indicated that, increasing the grinding time has a greater impact on the power consumption of iron ore ball milling than increasing the mill speed (Figure27). The calculated value of the Bond's (1952) mill power has been displayed on the table14.

Power(W)	Time(min)	Energy consumption(J)
1.11	5	5.55
1.11	15	16.65
1.11	25	27.75
1.11	35	38.85
1.11	45	49.95
1.11	65	66.6

Table 13: Shows the energy consumption of a ball mill operating at 450 rpm for various grinding times (5 to 60 minutes).

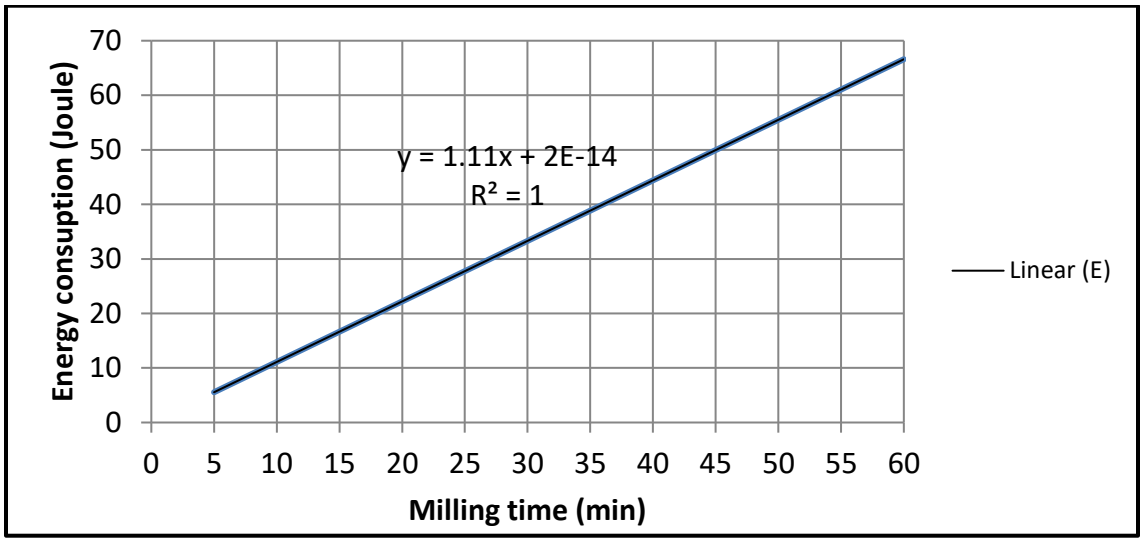

Figure 26: Shows mill energy consumption increment with longer milling time.

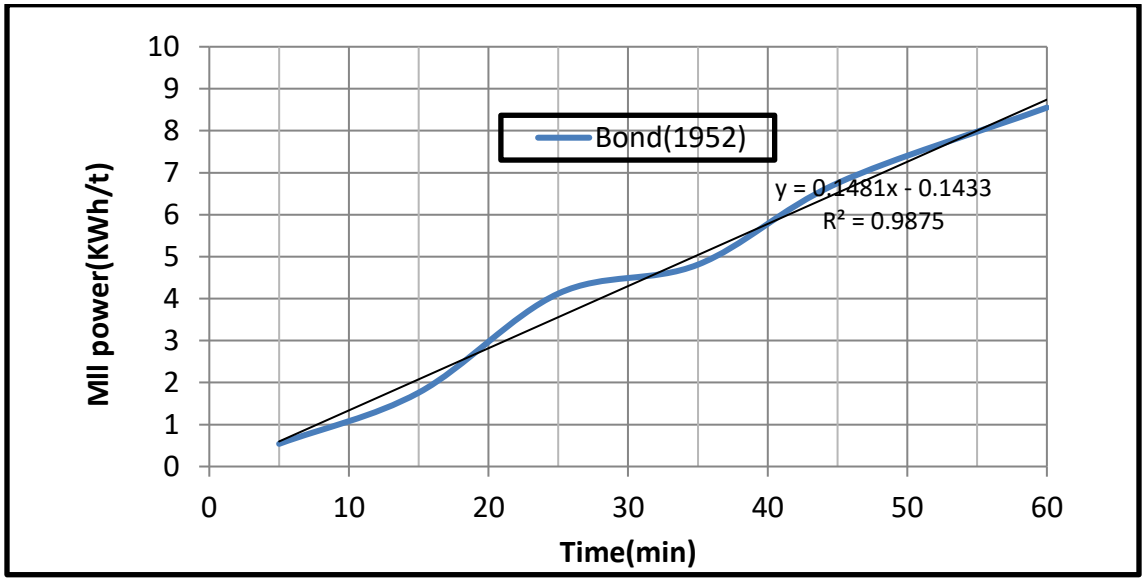

Figure 27: Variation of Bond's (1952) mill power with changing grinding time from 5 to 60 min.

Feed size(mm)	Time(min)	P80(µm)	Bond power(kWh/t)	Speed(rpm)	P(µm)	Bond power(kWh/t)
-3.35(bulk ore)	5	1870	0.54	250	1988	0.53
	15	978	1.76	300	1817	0.56
	25	413	4.12	350	226	1.68
	35	344	4.81	450	204	3.87
	45	218	6.75	550	666	1.13
	60	152	8.55	-	-	-

Table 14: the results of the grinding parameters of the -3.35mm iron ore feed size fraction.

5.1.3 Effect of feed size on grinding behavior of iron ore

1. Effect of feed size on Particle size distribution of milled products

. In the laboratory roller ball batch grinding test, the effects of changing the feed size (-3.35 + 0.71mm, -0.71+0.15mm, and -0.35mm), mill speed (250 to 550 rpm), and grinding time (5 to 60 min) on the particle size distribution results and abrasion behavior characteristics of the ground products were studied. Figures 28(a, b, and c) and Figure 29(a, b, and c) illustrate the variations in yield of target size (-0.075mm) and P80 with grinding time and mill rotational speed, respectively.

From Figure 28 and 29 it can be seen that slow milling is a low energy milling process and the particle size distribution of the product is non-uniform and tends to self-distribute into a second coarser fraction close to the original particle size of the feed itself and the fine fractions of -0.075mm, This indicates that the slow grinding process exhibited distinct abrasion behavior characteristics. Furthermore, it is concluded that the yield curves for all feed sizes shift upwards with increasing grinding time and mill rotational speed. When the relative particle size was fixed, the yield increased continuously, confirming that the slow grinding over time resulted in mineral comminution.

Even though the finer the grain size of the feed size has the greater the total surface area of minerals and the greater the effective contact area with the media and inner walls, the yield curves for ground products of the fine feed size show insignificant improvement. Comparing Figure 28 and 29 (a), (b) and(c) under the same grinding conditions, the variation of the product size distribution curve for feed size -0.71+0.15 mm for grinding and mill rotational speed was more unique than for -3.35 + 0.71 mm and -3.35 mm feed size fractions. Feed size -0.71+0.15 mm is less affected as grinding time rises from 5 to 60 min at low speed grinding (450 rpm), and mill speed increment from 250 to 450 rpm at 25 min .This suggested that it requires more energy to grind than other feed size fractions.

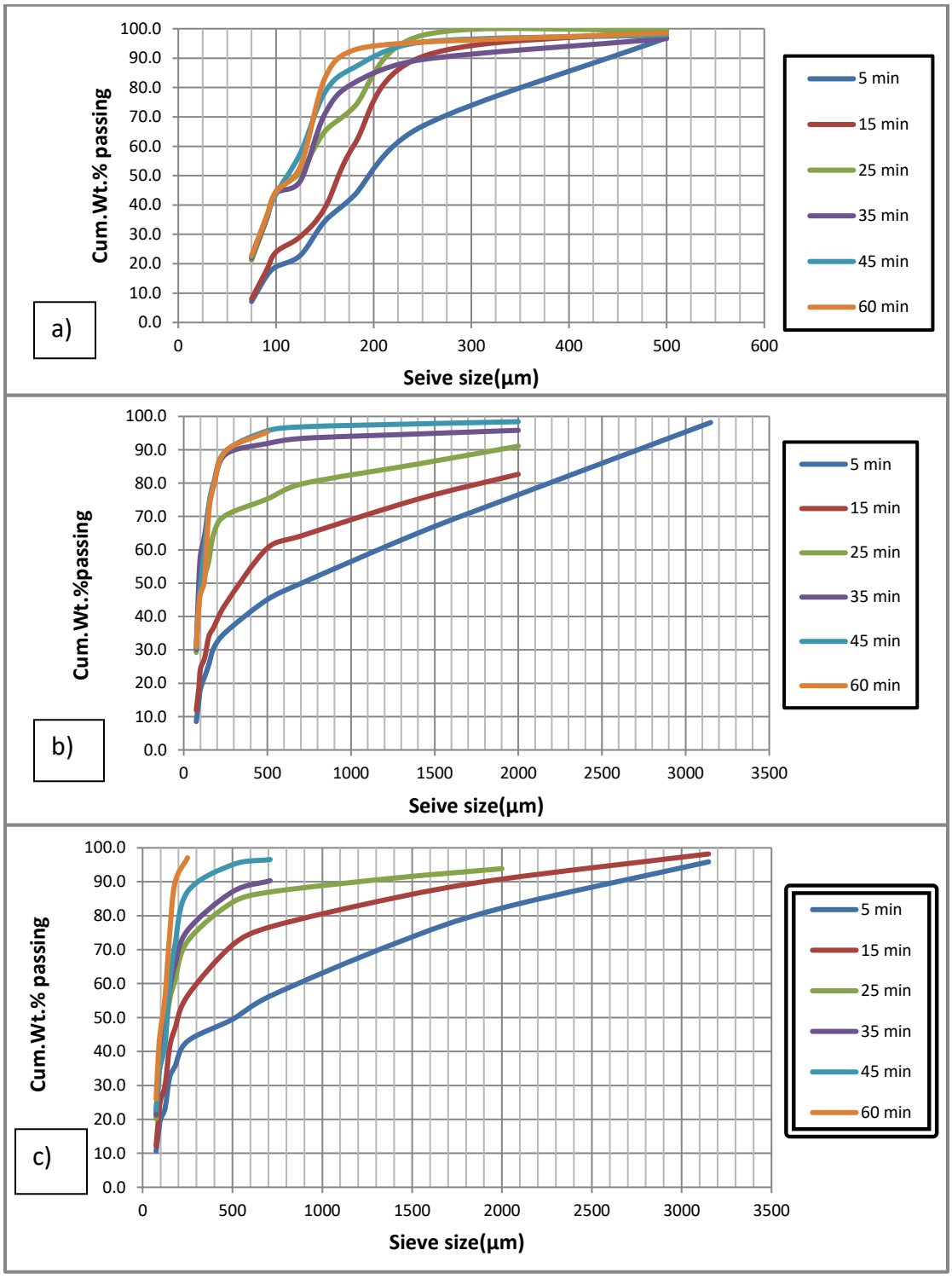

Figure 28:(a) product size distribution for -0.71+0.15mm ,(b) PSD for -3.35+0.71mm and (c) PSD for-3.35mm with varying grinding time from 5 to 60 min.

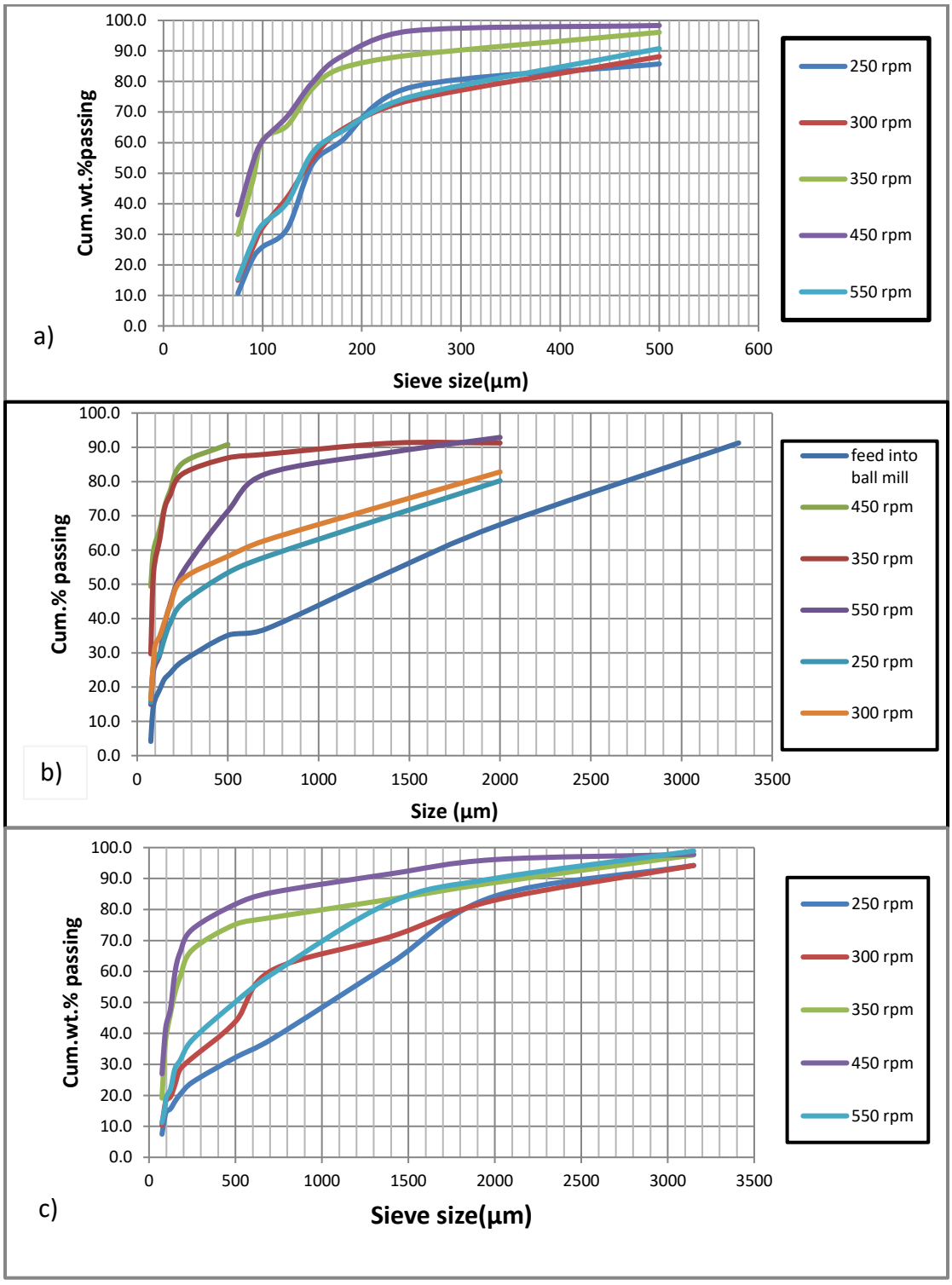

Figure 29(a,b&c): product size distribution curve for feed size;--0.71+0.15mm, 3.35+0.71mm and-3.35mm with changing mill speed from 250 to 550 rpm.

2) Interaction effect of grinding time and feed size

As shown in table15, the grinding time affect both the p80 and the percentage of the target size produced. As grinding time increased from 5 to 60 min, the amount of -0.075 mm is increased significantly in coarse feed size fraction but the p80 value is lower than the fine and mixed feed size. This indicated that at low speed grinding, fine feed size fractions are difficult to grind even grinding time increased significantly. The maximum amount of target size and p80 were 31.1% and 14 7 µm respectively The power drawn of the ball mill increased from 0.54 to 8.55 kWh/t as grinding time rises from 5 to 60 min for bulk feed size(-3.35mm) fractions(Table17). This indicated that longer grinding time cause higher amount of energy consumption especially in fine feed size without considerable amount of target size. As a result grinding time requires great emphasis than mill speed during grinding of the fine iron ore feed size.

Feed size/mm/	Time/min/	<0.075mm (%)	P80(µm)	Speed (rpm)
	5	8.5	2185	450
	15	11.9	1786	450
	25	29.2	731	450
-3.35+0.71	35	30.1	184	450
	45	30.6	178	450
	60	31.1	184	450
	5	7.1	359	450
	15	8.0	221	450
-0.71+0.15	25	21.2	199	450
	35	21.9	176	450
	45	22.4	156	450
	60	22.8	147	450
	5	10.6	1870	450
	15	12.2	978	450
-3.35	25	20.2	413	450
	35	21.3	344	450
	45	22.8	218	450
	60	26.0	152	450

Table 15: shows results of grinding parameters for milled iron ore particles at different grinding time.

3) Interaction effect of mill speed and feed size

Feed size/mm/	Mill speed/rpm/	<0.075mm (%)	P80(µm)	Time (min)
	250	7.5	1875	25
	300	10.3	1846	25
-3.35+0.71	350	19.1	1014	25
	450	27.0	448	25
	550	11.2	1329	25
	250	10.7	309	25
-0.71+0.15	300	14.9	357	25
	350	30.0	161	25
	450	36.4	151	25
	550	15.3	328	25
	250	15.5	1988	25
-3.35	300	16.5	1817	25
	350	29.7	226	25
	450	49.4	204	25
	550	14.9	666	25

Table 16: shows results of grinding parameters for milled iron ore particles at different mill speed.

Feed size(mm)	Time(min)	P80(µm)	Power(*)	Speed(rpm)	P(µm)	P(*)
	5	1870	0.54	250	1988	0.53
-3.35(bulk ore)	15	978	1.76	300	1817	0.56
	25	413	4.12	350	226	1.68
	35	344	4.81	450	204	3.87
	45	218	6.75	550	666	1.13
	60	152	8.55			

Table 17: shows the physical grinding specifications for -3.35mm iron ore feed size with changing grinding time and mill speed."*" indicates the unit of power(kWh/t).

From table16 and table17, the grinding processes of all feed sizes were affected with mill speed change. As mill speed increased from 250 to 450rpm, the amount of grind size increased from 7.5 to 49.4% and P80 decreased from 1875 to151µm. the power consumption is increased until maximum mill speed attained. 3.87 kWh/t is required to grind one tone of -3.35mm feed size at 450 rpm. This suggested that the iron ore is requires fine grinding mills (stirr- mills) that save power with considerable amount of grind size.

6. Conclusion and Recommendation

6.1 Conclusion

The purpose of this study was to investigate the effect of mill speed, grinding time and feed size on the product particle size distribution (p80 and target size) and the energy consumed in the iron ore grinding process. For each size fraction of the iron ore feed, a laboratory roller ball mill (150× 150 mm) was operated at five different speeds from 250 rpm to 550 rpm and at six different grinding times ranging from 5 to 60 minutes. The initial charge of the ball mill included different-sized balls (10 mm, 20 mm, and 27 mm) as well as 318 grams of raw material. Based on the interpretation of previous mineralogical studies and laboratory ball-milling analysis of Sekota iron ore, the following conclusions can be drawn.

In comparison to mill speed, milling time has a significant effect on the product size production of iron ore. The amount of desired product changes from 8.5 to 31.1%, 7.1 to 22.8%, and 10.6 to 26% as milling time increases from 5 to 60 minutes for coarse, fine, and bulk iron ore feed fractions, respectively. However, at maximum mill speed, the bulk iron ore feed size fraction generated 49.4% of the target size. Similarly, the P80 of product iron ore particles at the longest grinding time (60 min) reached 184, 147 and 152 µm. This suggests that the top size of iron ore feed particles is reduced to finer particles with increasing grinding time.

The target size amount was not achieved during grinding and was only achieved 49.4% for the bulk iron ore feed size fraction at 450 rpm. This suggests that the optimum grinding time and grinding speed have not been determined due to the intervention other operating variables such as the type of grinding medium and the mill charge volume.

The power drawn during the grinding process of coarse, fine, and bulk iron ore particles was affected by the grinding time and mill speed. As the grinding time increased from 5 to 60 minutes, the power consumption increased from 0.54 to 8.55 kWh/t, while the mill rotational speed increased from 250 to 450 rpm, the power consumption increased from 0.53 to 3.87 kWh/t. This demonstrated that grinding time has a greater impact on power consumption than mill rotational speed.

6.2 Recommendation

Based on the results of the present study the following recommendations are provided.

- -3.35 mm and -3.35+071 mm feed size fractions have provide better amount of grind size and P80 than fine feed size(-0.71+0.15mm).
- The desired amount of target size (-0.075 mm) were not obtained at this grinding operation. In ordered to achieve the desired size amount, the grinding media should be changed into steel ball.
- Grinding time has a greater influence on ball mill grinding efficiency than mill speed, changing power consumption from 0.54 to 8.55KWh/t. As a result, the ideal grinding time should be determined in order to reduce the effect on ball mill efficiency.
- The Sekota iron ore grinding process is assessed based on grinding time and mill speed, however multivariate analysis should be necessary to optimize the iron ore grinding performance in ball mills.
- To ascertain the operating speed and operation time for the iron ore grinding process, additional process mineralogical and comminution investigations are needed.

Reference

Akande and Adebayo (2013). Comparative Analysis of Grindability of Iron- ore and Granite. *Journal of Mining World Express Volume 2.*

Austin, L.G., Klimpel, R.R., 1984. Modeling for scale-up of tumbling ball mills: Control '84. J.A. Herbst (eds), Society of Mining Engineers of the American Institute of Mining, Metallurgical and Petroleum Engineers, New York, pp. 167–184.

Austin, L.G. A discussion of equations for the analysis of batch grinding data. *Powder Technol.* 1999, *106*, 71–77. [**Google Scholar**] [**CrossRef**]

Austin, L.G.; Luckie, P.T. The estimation of non-normalized breakage distribution parameters from batch grinding tests. *Powder Technol.* 1972, *5*, 267–270. [**Google Scholar**] [**CrossRef**

Austin, L.G.; Luckie, P.T. Methods for determination of breakage distribution parameters. *Powder Technol.* 1972, *5*, 215–222. [**Google Scholar**] [**CrossRef**]

Austin, L.G.; Klimpel, R.R.; Luckie, P.T. *Process Engineering of Size Reduction: Ball Milling*; Society of Mining Engineers of the American Institute of Mining, Metallurgical, and Petroleum Engineers: New York, NY, USA, 1984. [**Google Scholar**]

Banini, G.A. 2000. An integrated description of rock breakage in comminution machines. PhD Thesis, JKMRC, University of Queensland, Australia.

Belayneh.D.(2020).Mineralogy, Geochemistry, and Genesis of Mekane Selam iron ore occurrence in Tewa area, Northen Ethiopia. Unpublished MSc thesis in AAU.

Beukes N.J. and Klein C. (1992). Models for iron-formation deposition. The Proterozoic Biosphere (eds. J.W. Schopf and C. Klein), pp. 147–151. Cambridge, UK: Cambridge University Press. [A short but comprehensive overview of the formation of banded iron formations.]

Biswas, A. *Principles of Blast Furnace Iron Making*; Cootha: Calcutta, India, 2005. [**Google Scholar**].

Bond, F.C., 1949.Standard Grindibility test Tabuleted Trans. Am.Inst.Min.Eng.183:313-329.

Bond, F.C., 1952.Third Theory of Comminution Trans.Am.Inst.Min.Eng, 193:484-494.

Bond, F. C. (1961).Crushing and grinding calculations. *Br. Chem. Eng.* , *6*, 378–385. [**Google Scholar**]

Bourgeois, F.S. & Banini, G. A. 2002. A portable load cell for in-situ ore impact breakage testing. *International Journal of Mineral Processing*. **65**(1):31–54.

Cores, A.; Babich, A.; Muniz, M.; Isidro, A.; Ferreira, S.; Martin, R. Iron ores, fluxes and tuyere injected coals used in the blast furnace. *Ironmak. Steelmak.* 2007, *34*, 231–240. [**Google Scholar**] [**CrossRef**].

Dwari RK, Rao DS, Reddy PSR 2014 Mineralogical and Beneficiation Studies of a Low Grade Iron Ore Sample *J Inst Eng Ser D* **95** p115–23.

Geerdes, M.; Toxopeus, H.; van der Vliet, C.; Chaigneau, R.; Vander, T.; Wise, J. *Modern Blast Furnace Ironmaking: An Introduction*; IOS Press: Amsterdam, The Netherlands, 2009. [**Google Scholar**].

Gross, J. (1938). Crushing and grinding. Washington: united States gov. printing office.

GSE (2020).Mineral Exploration for Sekota iron ore deposit. Unpublished internal report. Addis Ababa,Ethipia.

Gupta, V. K., Sharma, S., 2014. Analysis of ball mill grinding operation using mill power specific kinetic parameters. Advanced Powder Technology, vol. 25, no. 2, pp. 265–634

Hahne, R., Pålsson, B.I. & Samskog, P.O. 2003. Ore characterisation for—and simulation of—primary autogenous grinding. *Minerals Engineering*. **16**(1):13–19.

Harish, H., Vardhan, H., Raj, M.G., Kaza, M., Sah, R., Sinha, A. and Kumar, S.B., 2020, January. Investigation of iron ores based on the bond grindability test. In *AIP Conference Proceedings* (Vol. 2204, No. 1, p. 040006). AIP Publishing LLC.

Hu, C., He, Y., Liu, D., Sun, S., Li, D., Zhu, Q. and Yu, J., 2019. Advances in mineral processing technologies related to iron, magnesium, and lithium. *Reviews in Chemical Engineering*, **36**(1), pp.107-146.

Mineral Commodities of Newfoundland and Labrador in Canada Geological Survey. *Iron Ore (*Number 7, 2012). [http://www.nr.gov.nl.ca/nr/mines/geoscience/:]

I. M. (July 07, 2016). Mineworx Files Patent on New Mineral Grinding Technology. Edmonton, Alberta.

Jankovic, A., 2015. Developments in iron ore comminution and classification technologies. *Iron Ore*, pp.251-282.

Kapur, P.C., Pande, D. & Fuerstenau, D.W. 1997. Analysis of single-particle breakage by impact grinding. **49**: 223–236.

Kick, F., 1885. Das Gezetz der proportionalen Winderstande und seine Anwendung. Arthur Felix, Leipzig.

King, R.P., 2001. *Modeling and simulation of mineral processing systems*. Elsevier.

Kwon, J. Simulation and optimization of a two-stage ball mill grinding circuit of molybdenum ore. *Adv. Powder Technol.* **2016**, *27*, 1073–1085. [**Google Scholar**] [**CrossRef**]

Kwon, J.; Cho, H.; Mun, M.; Kim, K. Modeling of coal breakage in a double-roll crusher considering the reagglomeration phenomena. *Powder Technol.* 2012, *232*, 113–123. [**Google Scholar**] [**CrossRef**]

Kwon, J. Investigation of breakage characteristics of low rank coals in a laboratory swing hammer mill. *Powder Technol.* **2014**, *256*, 377–384. [**Google Scholar**] [**CrossRef**][**Green Version**]

Krishna SJG, Patil MR, Rudrappa C, Kumar SP, Ravi BP 2013 Characterization and Processing of Some Iron Ores of India *J Inst Eng Ser D* **94** p113–20.

Larbi-Bram, S. 2009. A Study of Ore Breakage Characterization for AG/SAG Mill Modelling. University of Queensland.

Levin, J. 1992. Indicators of grindability and grinding efficiency. Journal of the South African Institute of Mining and Metallurgy, vol. 92, no. 10, pp. 283–290

Liao, J.L.; Li, J.; Wang, X.D.; Zhang, Z.T. Influence of TiO_2 and basicity on viscosity of Ti bearing slag. *Ironmak. Steelmak.* 2012, ***39,*** 133–139. [**Google Scholar**] [**CrossRef**].

Leung, K. 1987. An energy based ore specific model for autogenous and semiautogenous grinding. University of Queensland, Brisbane, Australia.

Lu, L.; Ishiyama, O. 2-Iron ore sintering. In *Iron Ore*; Lu, L., Ed.; *Woodhead Publishing:* Southton, UK, 2015; pp. 45–84. [**Google Scholar**].

Michaud, L. D. (January 2016). 911metallurgist: https://www.911metallurgist.com/conecrushers. Mining Energy Consumption (2021). A high-level study into mining energy use for the key mineral commodities of the future,[http://www.engeco.com.au/].

Muwanguzi, A.J.B.; Karasev, A.V.; Byaruhanga, J.K.; Jönsson, P.G. Characterization of Chemical Composition and Microstructure of Natural Iron Ore from Muko Deposits. *ISRN Mater. Sci.* 2012, *2012*, 1–9. [**Google Scholar**] [**CrossRef**][**Green Version**].

Mwanga, A., 2014. *Test Methods for Characterising Ore Comminution Behavior in Geometallurgy* (Doctoral dissertation, Luleå University of Technology).

Mwanga, Abdul, Pertti Lamberg, and Jan Rosenkranz. "Liberability: A new approach for measuring ore comminution behavior." *Process Mineralogy: 17/11/2014-19/11/2014*. 2014. Mwanga, A., Rosenkranz, J. and Lamberg, P., 2017. Development and experimental validation of the Geometallurgical Comminution Test (GCT). *Minerals Engineering*, *108*, pp.109-114. Reid, K.J. A solution to the batch grinding equation. *Chem. Eng. Sci.* **1965**, *20*, 953–963. [**Google Scholar**] [**CrossRef**]

Napier-Munn, T.J., Morell, S., Morrison, R.D. & Kojovic, T. 1996. Minerals Comminution Circuits: Their operation and optimization. *JKMRC*. Brisbane, Australia:

Napier-Mun, T. Is progress in energy-efficient comminution doomed? *Miner. Eng.* 2015, **73**, 1–6. [**Google Scholar] [CrossRef**].

Narayanan, S. 1985. Development of a Laboratory Single Particle Technique and its Application to Ball Mill Modeling and Scale up. University of Queensland, Brisbane, Australia.

SGS Minerals, 2005. An Overview of the Small-scale Tests Available to Characterize Ore Grindability for Design Purpose[http://www.sgs.com/minerals]

Shi, F. & Kojovic, T. 2007. Validation of a model for impact breakage incorporating particle size effect. *International Journal of Mineral Processing*. 82(3):156–163.

SMP, 2016.Feasibility study on large scale Sekota iron ore, in mining. Ministry of Mine, Ethiopia.

Starkey and Dobby G. (1996) "Application of the SAG Power Index at Five Canadian SAG Plants." Proceedings Autogenous and Semiautogenous Grinding 1996, UBC, Vancouver, BC

Song, S.-X.; Campos-Toro, E.F.; Zhang, Y.-M.; Lopez-Valdivieso, A. Morphological and mineralogical characterizations of oolitic iron ore in the Exi region, China. *Int. J. Miner. Met. Mater.* **2013**, ***20***, 113–118. [**Google Scholar**] [**CrossRef**].

Stambodiadis, E., Emmanaoilidis S., Petrakis E.A., 2011. New approach to the calculation of work index and the potential energy of a particulate material. Geomaterisld, vol. 1, pp. 20–32

Tavares, L.M. 2007. Breakage of Single Particles: Quasi-Static. In Particle Breakage: *Handbook of PowderTechnology*. 12. A.D. Salman, M. Ghadiri, & M.J. Hounslow, Eds. Amsterdam: Elsevier Science & Technology Books. 3–68.

Tøgersen, M.K., Kleiv, R.A., Ellefmo, S. and Aasly, K., 2018. Mineralogy and texture of the Storforshei iron formation, and their effect on grindability. *Minerals Engineering*, *125*, pp.176-189.

Tavares, L. & King, R. 1998. Single-particle fracture under impact loading. *International Journal of Mineral Processing*. **54**(1):1–28.

U.S Geological Survey, Mineral Commodity Summaries 2022, [2022-10-21]. https://doi.org/ 10.3133/mcs2022.

Wakelin, D.H. *The Making, Shaping and Treating of Steel: Ironmaking Volume*; AISE Steel Foundation: Pittsburgh, PA, USA, 1999. [**Google Scholar**].

Williams, N.R. & Holtzhausen, S. 2001. The impact of ore characterization and blending on metallurgical plant performance: 437–446.

Wills, B.A., 1990. Comminution in the minerals industry-an overview. *Minerals Engineering*, **3**(1-2), pp.3-5.

Wills, B.A., 1998. *Mineral Processing Technology*, Pergamon Press, England, 460.

Wills, B.A. & Napier-Munn, T. 2006. *Mineral Processing Technology*. *7th Edition*. Elsevier Science & Technology Books.

Appendixes

Appendix A: Optical Microscope images of Sekota iron ore sample (SMP2016).

Figure 1 Photo-micrograph shows bands of Goethite(G) as highly altered product of Hematite(H). Few minute grains of Hematite(H) also present in the ground mass. [Under Transmitted light_50x].

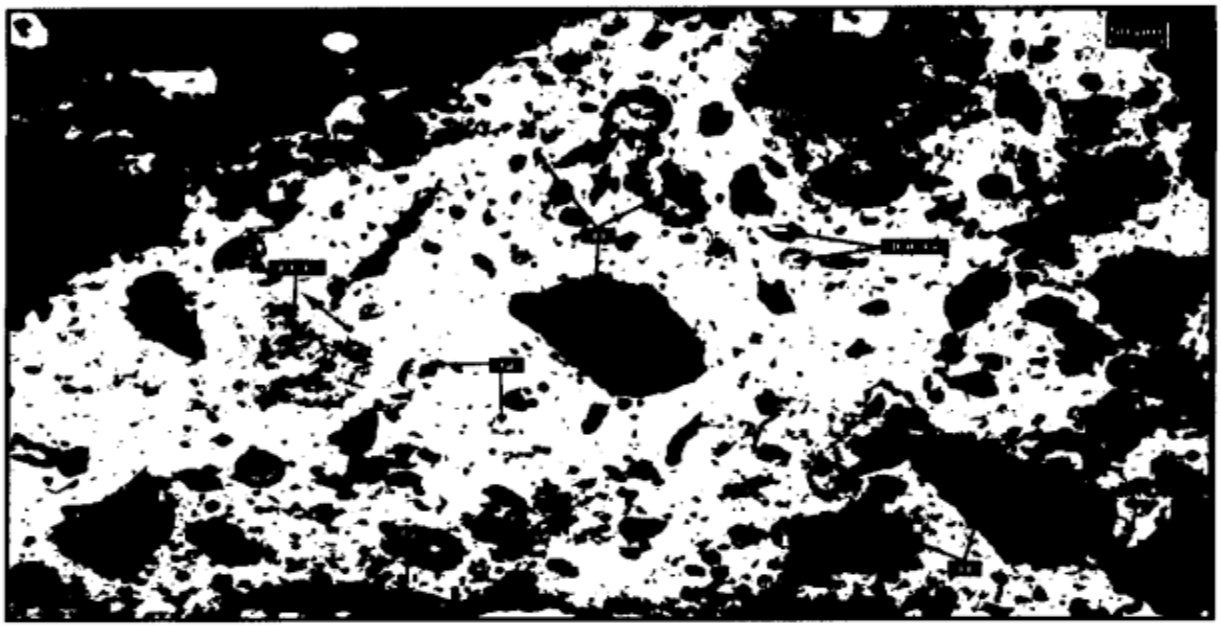

Figure 2 Photo-micrograph shows irregular shaped remnant grains of Hematite(H) and few altered product Goethite(G). Few minute grains of Quartz(Q) and Iron Ore Coated Gangue(IOCG) also observed. Ferruginous Clay(FCL) occurs at ground mass. [Under Transmitted light_100x].

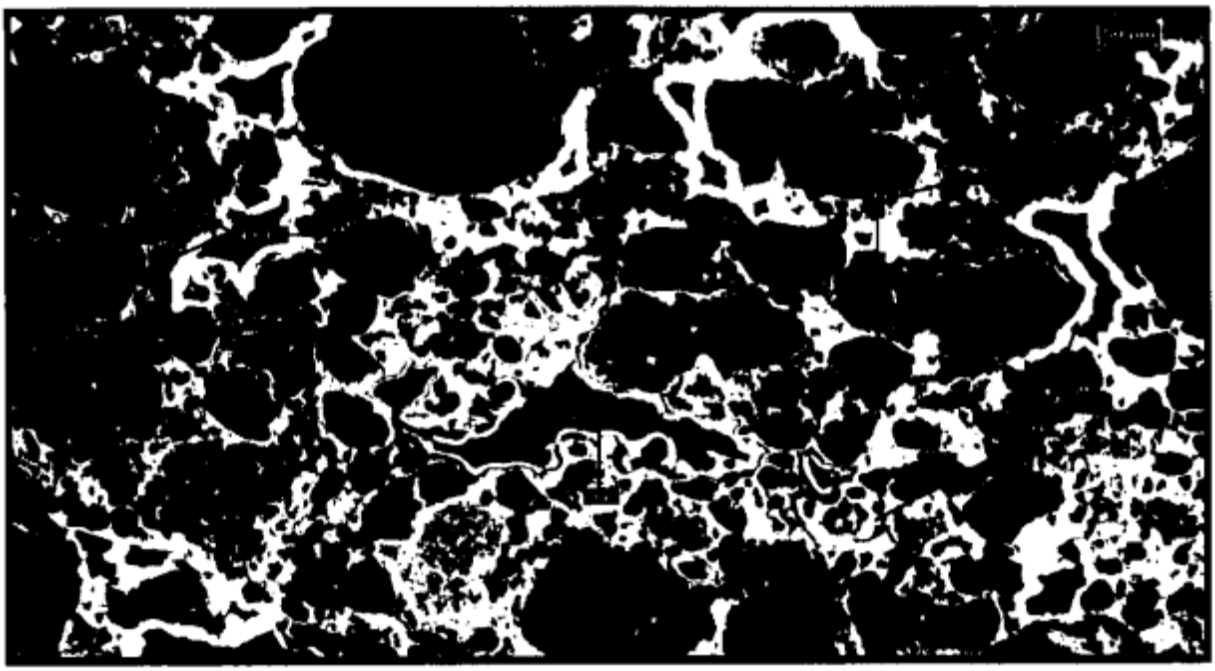

Figure 3 Photo-micrograph depicts highly altered iron ore. Bends of Hematite(H), its altered product Goethite(G) with colloform texture. Ferruginous Clay(FCL) occurs at ground mass. Few quartz(Q) also present. [Under Reflected light_100x].

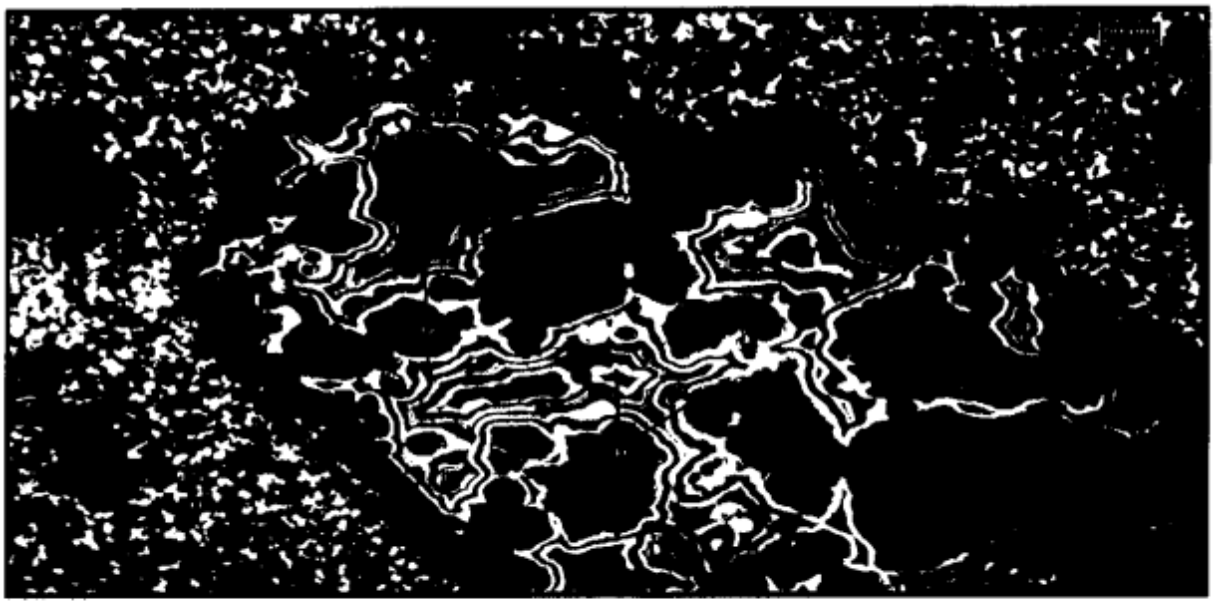

Figure 4 Photo-micrograph shows colloform banding as alteration structure. Bands of Hematite(H) and Goethite(G) present. Minute grains of altered Hematite(H) also present. Few Quartz(Q) and Ferruginous Clay(FCL) occurs at ground mass. [Under Reflected light_100x].

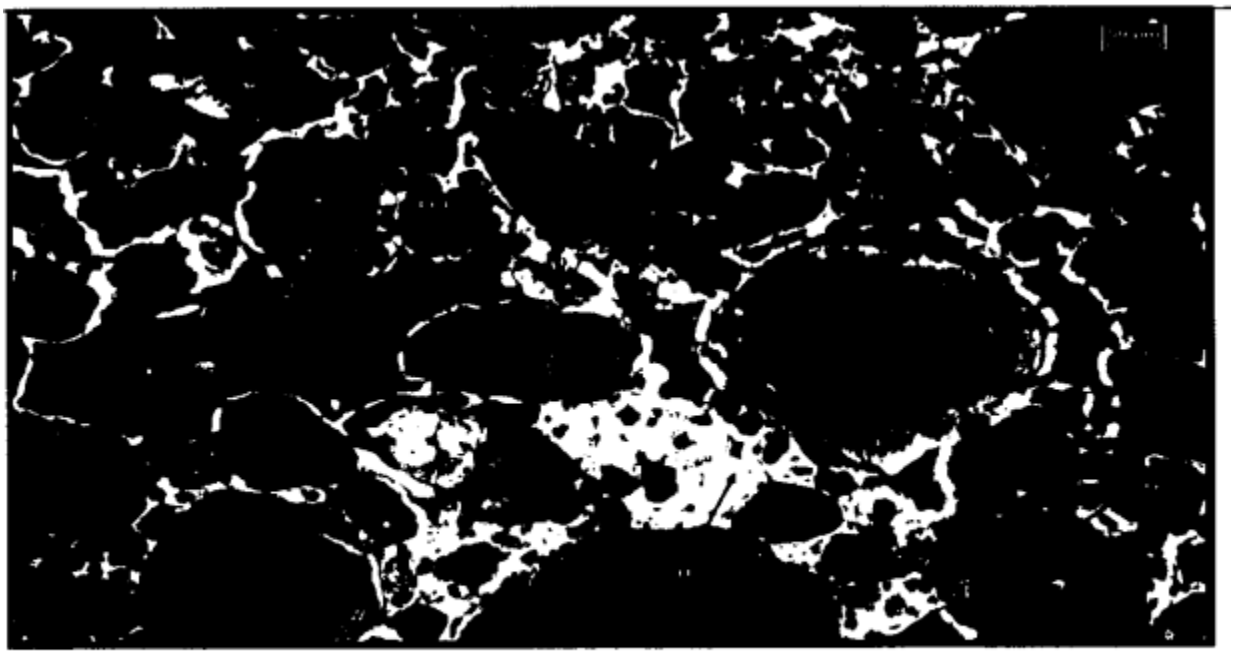

Figure 5 Photo-micrograph depicts highly altered iron ore. Irregular shaped Hematite(H) occurs as grain margins. Altered product Goethite(G) occurs at core of primary mineral grains. Few irregular shaped Quartz(Q) also occurs as. Ferruginous Clay(FCL) occurs at [Under Reflected light_100x].

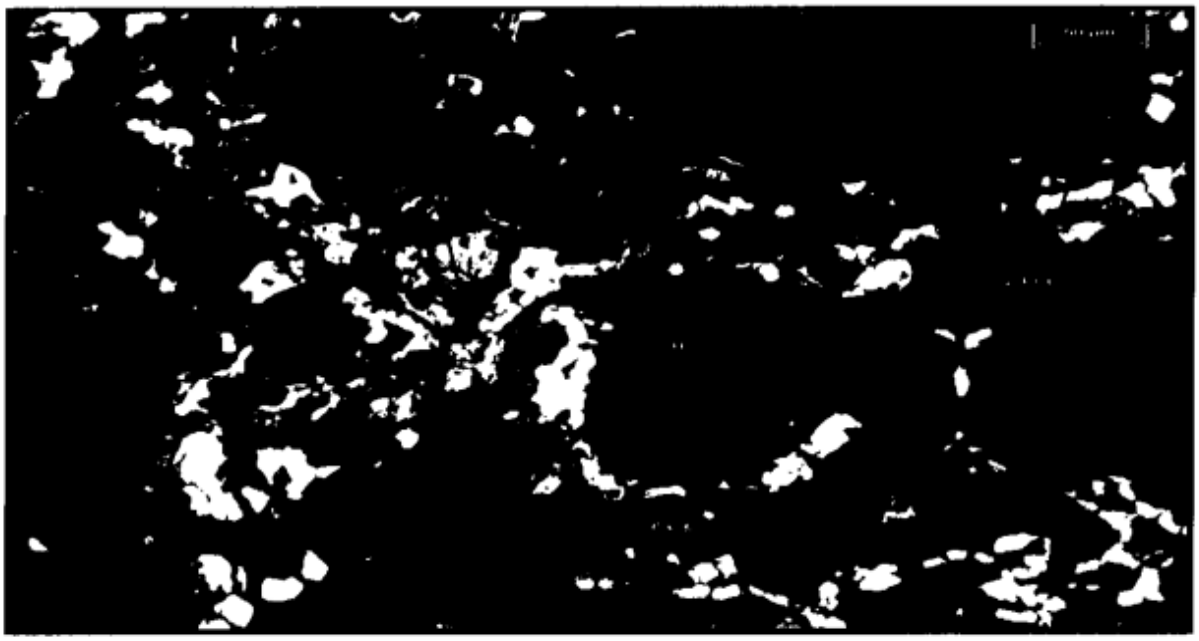

Figure 6 Photo-micrograph shows highly altered iron ore with remnant structure of colloform bands. Few irregular shaped Hematite(H) and Quartz(Q) shown in the image. Ferruginous Clay(FCL) at ground mass. [Under Transmitted light_200x].

Appendix B: Product size distribution of Sekota iron ore sample at different grinding time.

For feed size -3.35+0.71mm						
at 5 min with 450 rpm						
sieve size(µm)	sieve weight(g)	Sieve +sample (g)	weight retained (g)	Weight retained (%)	cum.wt.% passing	cum.wt. % retained
3150	370.6	376.4	5.8	1.8	98.2	1.8
2000	334	403.2	69.2	21.7	76.5	23.5
1400	321.8	358.6	36.8	11.5	65.0	35.0
710	290.3	337.8	47.5	14.9	50.1	49.9
500	483.6	499.7	16.1	5.0	45.1	54.9
250	250.7	282.1	31.4	9.8	35.3	64.7
180	278	292.8	14.8	4.6	30.6	69.4
150	241.5	257.7	16.2	5.1	25.6	74.4
125	276.2	287.8	11.6	3.6	21.9	78.1
100	255.5	267	11.5	3.6	18.3	81.7
90	355.5	367.4	11.9	3.7	14.6	85.4
75	287.1	306.6	19.5	6.1	8.5	91.5
-75	240.2	267.4	27.2	8.5	0.0	100.0
total			**319.5**	**100.0**	**100.0**	
at 15 min with 450 rpm						
sieve size(µm)	sieve weight (g)	Sieve + sample (g)	weight retained(g)	Weight retained (%)	cum.wt.% passing	cum.% retained
2000	334	389.1	55.1	17.3	82.7	17.3
1400	321.8	345.5	23.7	7.5	75.2	24.8
710	290.3	324.9	34.6	10.9	64.3	35.7
500	483.6	495.6	12	3.8	60.5	39.5
250	250.7	304.1	53.4	16.8	43.7	56.3
180	278	299.9	21.9	6.9	36.8	63.2
150	241.5	250.4	8.9	2.8	34.0	66.0
125	276.2	296.6	20.4	6.4	27.6	72.4
100	255.5	266	10.5	3.3	24.3	75.7
90	355.5	374	18.5	5.8	18.5	81.5
75	287.1	308	20.9	6.6	11.9	88.1
-75	240.2	278	37.8	11.9	0.0	100.0
			317.7	100.0		
at 25 min 450 rpm						
sieve size(µm)	sieve weight(g)	Sieve + sample(g)	weight retained(g)	Weight retained (%)	cum.wt.% passing	cum.% retained
2000	334	362.3	28.3	8.9	91.1	8.9
1400	321.8	338.8	17	5.4	85.7	14.3
710	290.3	309.1	18.8	5.9	79.8	20.2

500	483.6	490.6	14.5	4.6	75.3	24.7
250	250.7	266.4	15.7	4.9	70.3	29.7
180	278	295.1	17.1	5.4	64.9	35.1
150	241.5	256.2	26.3	8.3	56.6	43.4
125	276.2	290.8	14.6	4.6	52.0	48.0
90	355.5	381.2	25.7	8.1	44.0	56.0
75	287.1	333.9	46.8	14.7	29.2	70.8
-75	240.2	333	92.8	29.2	0.0	100.0
total			**317.6**	**100.0**		
at 35 min with 450 rpm						
sieve size(µm)	sieve weight(g)	Sieve+ sample(g)	weight retained(g)	Weight retained (%)	cum.wt.% passing	cum.% retained
2000	334	347.2	13.2	4.2	95.8	4.2
1400	321.8	325.3	3.5	1.1	94.7	5.3
710	290.3	294.5	4.2	1.3	93.4	6.6
500	483.6	488.5	4.9	1.5	91.9	8.1
250	250.7	261	10.3	3.2	88.6	11.4
180	278	307.3	29.3	9.2	79.4	20.6
150	241.5	261.5	20	6.3	73.1	26.9
125	276.2	304.1	27.9	8.8	64.3	35.7
100	255.5	274.3	18.8	5.9	58.4	41.6
90	355.5	381.3	25.8	8.1	50.3	49.7
75	287.1	351.4	64.3	20.2	30.1	69.9
-75	240.2	335.8	95.6	30.1	0.0	100.0
total			**317.8**	100.0		
at 45 min with 450 rpm						
sieve size(µm)	sieve weight(g)	Sieve+ sample(g)	weight retained(g)	Weight retained (%)	cum.wt.% passing	cum.% retained
2000	334	339	5	1.6	98.4	1.6
1400	321.8	323.9	2.1	0.7	97.8	2.2
710	290.3	293.1	2.8	0.9	96.9	3.1
500	483.6	487.4	3.8	1.2	95.7	4.3
250	250.7	270.1	19.4	6.1	89.6	10.4
180	278	307.1	29.1	9.2	80.4	19.6
150	241.5	263.7	22.2	7.0	73.4	26.6
125	276.2	317	40.8	12.8	60.6	39.4
100	255.5	292	36.5	11.5	49.1	50.9
90	355.5	373.9	18.4	5.8	43.3	56.7
75	287.1	327.3	40.2	12.7	30.6	69.4
-75	240.2	337.5	97.3	30.6	0.0	100.0
total			**317.6**	100.0		
at 60 min with 450 rpm						

sieve size(µm)	sieve weight(g)	Sieve+sample(g)	weight retained(g)	Weight retained (%)	cum.wt.% passing	cum.% retained
500	483.6	498.4	14.8	4.7	95.3	4.7
250	250.7	268.9	18.2	5.7	89.6	10.4
180	278	310.3	32.3	10.2	79.4	20.6
150	241.5	267	25.5	8.0	71.4	28.6
125	276.2	341.3	65.1	20.5	50.9	49.1
100	255.5	268.1	12.6	4.0	46.9	53.1
90	355.5	368.4	12.6	4.0	42.9	57.1
75	287.1	326.1	37.6	11.8	31.1	68.9
-75	240.2	338.8	98.6	31.1	0.0	100.0
total			**317.3**	**100.0**		

For Feed Size -0.71 To+0.15mm						
at 5 min with 450 rpm						
sieve size(µm)	sieve weight(g)	Sieve+ sample(g)	weight retained(g)	Weight retained (%)	cum.wt.% passing	cum.% retained
500	483.6	493.4	9.8	3.1	96.9	3.1
250	250.7	346.3	95.6	30.1	66.8	33.2
180	278	353.1	75.1	23.6	43.2	56.8
150	241.5	269.3	27.8	8.7	34.5	65.5
125	276.2	313.1	36.9	11.6	22.9	77.1
100	255.5	268	12.5	3.9	18.9	81.1
90	355.5	366	10.5	3.3	15.6	84.4
75	287.1	314.2	27.1	8.5	7.1	92.9
-75	240.2	262.8	22.6	7.1	0.0	100.0
total			**317.9**	**100.0**		
at 15 min with 450 rpm						
sieve size(µm)	sieve weight(g)	Sieve+ sample(g)	weight retained(g)	Weight retained (%)	cum.wt.% passing	cum.% retained
500	483.6	485.5	1.9	0.6	99.4	0.6
250	250.7	278.9	28.2	8.9	90.5	9.5
180	278	373.6	95.6	30.1	60.4	39.6
150	241.5	309.7	68.2	21.5	38.9	61.1
125	276.2	307	30.8	9.7	29.3	70.7
100	255.5	272.3	16.8	5.3	24.0	76.0
90	355.5	375.8	20.3	6.4	17.6	82.4
75	287.1	317.4	30.3	9.5	8.0	92.0
-75	240.2	265.7	25.5	8.0	0.0	100.0
total			**317.6**	**100**		
at 25 min 450 rpm						
sieve	sieve	Sieve+	weight	Weight	cum.wt.%	cum.%

size(µm)	weight(g)	sample(g)	retained(g)	retained (%)	passing	retained
500	483.6	485.1	1.5	0.5	99.5	0.5
250	250.7	256.3	5.6	1.8	97.8	2.2
180	278	355.6	77.6	24.4	73.3	26.7
150	241.5	268	26.5	8.3	65.0	35.0
125	276.2	320	43.8	13.8	51.2	48.8
100	255.5	276.5	21	6.6	44.6	55.4
90	355.5	387	31.5	9.9	34.7	65.3
75	287.1	329.9	42.8	13.5	21.2	78.8
-75	240.2	307.7	67.5	21.2	0.0	100.0
total			**317.8**	**100**		
at 35 min with 450 rpm						
sieve size(µm)	sieve weight(g)	Sieve +sample(g)	weight retained(g)	Weight retained (%)	cum.wt.% passing	cum.% retained
500	483.6	494.2	10.6	3.3	96.7	3.3
250	250.7	273.4	22.7	7.1	89.5	10.5
180	278	303.2	25.2	7.9	81.6	18.4
150	241.5	275.2	33.7	10.6	71.0	29.0
125	276.2	348.5	72.3	22.8	48.2	51.8
100	255.5	269.0	13.5	4.3	44.0	56.0
90	355.5	384	28.5	9.0	35.0	65.0
75	287.1	328.6	41.5	13.1	21.9	78.1
-75	240.2	309.8	69.6	21.9	0.0	100.0
			317.6	100.0		
at 45 min with 450 rpm						
sieve size(µm)	sieve weight(g)	Sieve+ sample(g)	weight retained(g)	Weight retained (%)	cum.wt.% passing	cum.% retained
500	483.6	490.3	6.7	2.1	97.9	2.1
250	250.7	258.4	7.7	2.4	95.5	4.5
180	278	305.5	27.5	8.7	86.8	13.2
150	241.5	268.5	27	8.5	78.3	21.7
125	276.2	341.6	65.4	20.6	57.7	42.3
100	255.5	299.6	44.1	13.9	43.8	56.2
90	355.5	381.3	25.8	8.1	35.6	64.4
75	287.1	329.2	42.1	13.3	22.4	77.6
-75	240.2	311.1	70.9	22.4	0.0	100.0
total			**317.2**	100.0		
at 60 min with 450 rpm						
sieve size(µm)	sieve weight(g)	Sieve+ sample(g)	weight retained(g)	Weight retained (%)	cum.wt.% passing	cum.% retained
500	483.6	488.3	4.7	1.5	98.5	1.5
250	250.7	260.5	9.8	3.1	95.4	4.6

180	278	286.5	8.5	2.7	92.8	7.2
150	241.5	272.2	30.7	9.7	83.1	16.9
125	276.2	371.5	95.3	30.0	53.1	46.9
100	255.5	282.9	27.4	8.6	44.5	55.5
90	355.5	383.3	27.8	8.7	35.7	64.3
75	287.1	328.3	41.2	13.0	22.8	77.2
-75	240.2	312.6	72.4	22.8	0.0	100.0
			317.8	**100.0**		-

product size distribution for bulk						
at 5 min with 450 rpm						
sieve size(µm)	sieve weight (g)	Sieve+ sample(g)	weight retained(g)	Weight retained (%)	cum.wt.% passing	cum.% retained
3150	370.6	383.7	13.1	4.1	95.9	4.1
2000	334	377.2	43.2	13.6	82.3	17.7
1400	321.8	355.3	33.5	10.5	71.7	28.3
710	290.3	339.2	48.9	15.4	56.3	43.7
500	483.6	505.4	21.8	6.9	49.5	50.5
250	250.7	271.2	20.5	6.5	43.0	57.0
180	278	301.6	23.6	7.4	35.6	64.4
150	241.5	252	10.5	3.3	32.3	67.7
125	276.2	304.8	28.6	9.0	23.3	76.7
100	255.5	265.7	10.2	3.2	20.1	79.9
90	355.5	366	10.5	3.3	16.8	83.2
75	287.1	306.6	19.5	6.1	10.6	89.4
-75	240.2	274	33.8	10.6	0.0	100.0
			317.7	100.0		
at 15 min with 450 rpm						
sieve size(µm)	sieve weight(g)	Sieve+ sample(g)	weight retained(g)	Weight retained (%)	cum.wt.% passing	cum.% retained
3150	370.6	376.3	5.7	1.8	98.2	1.8
2000	334	357.5	23.5	7.4	90.8	9.2
1400	321.8	339.5	17.7	5.6	85.2	14.8
710	290.3	317.4	27.1	8.5	76.7	23.3
500	483.6	500.5	16.9	5.3	71.4	28.6
250	250.7	298.2	47.5	15.0	56.4	43.6
180	278	308.7	30.7	9.7	46.8	53.2
150	241.5	259.3	17.8	5.6	41.2	58.8
125	276.2	311.6	35.4	11.1	30.0	70.0
100	255.5	268.9	13.4	4.2	25.8	74.2
90	355.5	369.2	13.7	4.3	21.5	78.5

75	287.1	316.7	29.6	9.3	12.2	87.8
-75	240.2	278.8	38.6	12.2	0.0	100.0
total			317.6	100.0		
at 25 min with 450 rpm						
sieve size(µm)	sieve weight(g)	Sieve+ sample (g)	weight retained(g)	weight retained(%)	cum.wt.% passing	cum.wt.% retained
2000	334	353.5	19.5	6.1	93.9	6.1
1400	321.8	330.6	8.8	2.8	91.1	8.9
710	290.3	303.3	13	4.1	87.0	13.0
500	483.6	493.3	9.7	3.1	84.0	16.0
250	250.7	287.2	36.5	11.5	72.5	27.5
180	278	314.9	36.9	11.6	60.9	39.1
150	241.5	259.7	18.2	5.7	55.1	44.9
125	276.2	307.5	31.3	9.8	45.3	54.7
100	255.5	276.6	21.1	6.6	38.6	61.4
90	355.5	370.7	15.2	4.8	33.9	66.1
75	287.1	330.6	43.5	13.7	20.2	79.8
-75	240.2	304.3	64.1	20.2	0.0	100.0
			317.8	100		
at 35 min with 450 rpm						
sieve size(µm)	sieve weight(g)	Sieve +sample(g)	weight retained(g)	Weight retained (%)	cum.wt.% passing	cum.% retained
710	290.3	321	30.7	9.7	90.3	9.7
500	483.6	494	10.4	3.3	87.1	12.9
250	250.7	286.8	36.1	11.4	75.7	24.3
180	278	310.5	32.5	10.2	65.5	34.5
150	241.5	265.5	24	7.6	57.9	42.1
125	276.2	311.5	35.3	11.1	46.8	53.2
100	255.5	283.7	28.2	8.9	37.9	62.1
90	355.5	366.9	11.4	3.6	34.3	65.7
75	287.1	328.6	41.5	13.1	21.3	78.7
-75	240.2	307.7	67.5	21.3	0.0	100.0
			317.6	100.0		
at 45 min with 450 rpm						
sieve size(µm)	sieve weight(g)	Sieve +sample(g)	weight retained(g)	Weight retained (%)	cum.wt.% passing	cum.% retained
710	290.3	301.2	10.9	3.4	96.6	3.4
500	483.6	488.5	4.9	1.5	95.0	5.0
250	250.7	275.9	25.2	7.9	87.1	12.9
180	278	327.8	49.8	15.7	71.4	28.6
150	241.5	279.4	37.9	11.9	59.5	40.5
125	276.2	331.3	55.1	17.3	42.2	57.8
100	255.5	274.8	19.3	6.1	36.1	63.9

90	355.5	365.7	10.2	3.2	32.9	67.1
75	287.1	319.1	32	10.1	22.8	77.2
-75	240.2	312.7	72.5	22.8	0.0	100.0
			317.8	100.0		
at 60 min with 450 rpm						
sieve size(µm)	sieve weight (g)	Sieve+ sample (g)	weight retained(g)	Weight retained (%)	cum.wt.% passing	cum.wt. % retained
250	250.7	260	9.3	2.9	97.1	2.9
180	278	301.5	23.5	7.4	89.7	10.3
150	241.5	290.9	49.4	15.5	74.1	25.9
125	276.2	333.1	56.9	17.9	56.2	43.8
100	255.5	287	31.5	9.9	46.3	53.7
90	355.5	371.7	16.2	5.1	41.2	58.8
75	287.1	335.6	48.5	15.3	26.0	74.0
-75	240.2	322.8	82.6	26.0	0.0	100.0
Total			317.9	100.0		

Appendix C: Product size distribution of Sekota iron ore sample at different mill speed

product size distribution for -3.355+0.71 mm						
at 250 rpm with 25 min						
sieve size(µm)	sieve weight(g)	Sieve+ sample(g)	weight retained(g)	Weight retained (%)	cum.wt.% passing	cum.% retained
3150	370.6	389	18.4	5.8	94.2	5.8
2000	334	365.5	31.5	9.9	84.3	15.7
1400	321.8	390.5	68.7	21.6	62.7	37.3
710	290.3	368.5	78.2	24.6	38.2	61.8
500	483.6	502.4	18.8	5.9	32.3	67.7
250	250.7	276.3	25.6	8.0	24.2	75.8
180	278	290.5	12.5	3.9	20.3	79.7
150	241.5	248.7	7.2	2.3	18.0	82.0
125	276.2	283.5	7.3	2.3	15.7	84.3
100	255.5	258.8	3.3	1.0	14.7	85.3
90	355.5	362	6.5	2.0	12.7	87.3
75	287.1	303.6	16.5	5.2	7.5	92.5
-75	240.2	264	23.8	7.5	0.0	100.0
			318.3	100.0		
at 300 rpm with 25 min						
sieve size(µm)	sieve weight(g)	Sieve+ sample(g)	weight retained(g)	Weight retained (%)	cum.wt.% passing	cum.% retained
3150	370.6	389	18.4	5.8	94.2	5.8
2000	334	369.6	35.6	11.2	83.0	17.0
1400	321.8	359.1	37.3	11.7	71.3	28.7

710	290.3	325	34.7	10.9	60.4	39.6
500	483.6	536.1	52.5	16.5	43.9	56.1
250	250.7	288	37.3	11.7	32.1	67.9
180	278	289.7	11.7	3.7	28.4	71.6
150	241.5	257.3	15.8	5.0	23.5	76.5
125	276.2	288.3	12.1	3.8	19.7	80.3
100	255.5	259.3	3.8	1.2	18.5	81.5
90	355.5	362.7	7.2	2.3	16.2	83.8
75	287.1	305.8	18.7	5.9	10.3	89.7
-75	240.2	273	32.8	10.3	0.0	100.0
total			317.9	100.0		
at 350 rpm with 25 min						
sieve size(µm)	sieve weight(g)	Sieve+ sample(g)	weight retained(g)	weight retained(%)	cum.wt.% passing	cum.% retained
3150	370.6	378.2	7.6	2.4	97.6	2.4
2000	334	362.3	28.3	8.9	88.7	11.3
1400	321.8	338.8	17	5.4	83.3	16.7
710	290.3	309.1	18.8	5.9	77.4	22.6
500	483.6	490.6	7	2.2	75.2	24.8
250	250.7	276.9	26.2	8.2	67.0	33.0
180	278	305.7	27.7	8.7	58.2	41.8
150	241.5	257.8	16.3	5.1	53.1	46.9
125	276.2	296.9	20.7	6.5	46.6	53.4
100	255.5	277.8	22.3	7.0	39.6	60.4
90	355.5	373.7	18.2	5.7	33.8	66.2
75	287.1	333.9	46.8	14.7	19.1	80.9
-75	240.2	300.9	60.7	19.1	0.0	100.0
total			317.6	100.0		
at 450 rpm with 25 min						
sieve size(µm)	sieve weight(g)	Sieve+ sample(g)	weight retained(g)	Weight retained (%)	cum.wt.% passing	cum.% retained
3150	370.6	377.6	7	2.2	97.8	2.2
2000	334	339.3	5.3	1.7	96.1	3.9
1400	321.8	336.3	14.5	4.6	91.6	8.4
710	290.3	309.6	19.3	6.1	85.5	14.5
500	483.6	495.5	11.9	3.7	81.7	18.3
250	250.7	276.4	25.7	8.1	73.6	26.4
180	278	301.5	23.5	7.4	66.2	33.8
150	241.5	262.2	20.7	6.5	59.7	40.3
125	276.2	312.6	36.4	11.5	48.2	51.8
100	255.5	272.2	16.7	5.3	43.0	57.0
90	355.5	371.1	15.6	4.9	38.1	61.9

75	287.1	322.3	35.2	11.1	27.0	73.0
-75	240.2	325.8	85.6	27.0	0.0	100.0
total			317.4	100.0		
at 550 rpm with 25 min						
sieve size(µm)	sieve weight(g)	Sieve+ sample(g)	weight retained(g)	Weight retained (%)	cum.wt.% passing	cum.% retained
3150	370.6	374.1	3.5	1.1	98.9	1.1
2000	334	362.1	28.1	8.8	90.1	9.9
1400	321.8	346.1	24.3	7.6	82.4	17.6
710	290.3	364.3	74	23.3	59.1	40.9
500	483.6	512.1	28.5	9.0	50.2	49.8
250	250.7	289.6	38.9	12.2	37.9	62.1
180	278	299	21	6.6	31.3	68.7
150	241.5	249.9	8.4	2.6	28.7	71.3
125	276.2	296.8	20.6	6.5	22.2	77.8
100	255.5	264	8.5	2.7	19.5	80.5
90	355.5	368.7	13.2	4.2	15.4	84.6
75	287.1	300.3	13.2	4.2	11.2	88.8
-75	240.2	275.8	35.6	11.2	0.0	100.0
			317.8	100.0		

product size distribution for -0.71+0.15mm						
at 250 rpm with 25 min						
sieve size(µm)	sieve weight(g)	Sieve+ sample(g)	weight retained(g)	Weight retained (%)	cum.wt.% passing	cum.% retained
500	483.6	528.9	45.3	14.2	85.8	14.2
250	250.7	274.9	24.2	7.6	78.2	21.8
180	278	333.7	55.7	17.5	60.6	39.4
150	241.5	266.2	24.7	7.8	52.9	47.1
125	276.2	342.9	66.7	21.0	31.9	68.1
100	255.5	274.7	19.2	6.0	25.9	74.1
90	355.5	367.6	12.1	3.8	22.1	77.9
75	287.1	323.4	36.3	11.4	10.7	89.3
pan	240.2	274.1	33.9	10.7	0.0	100.0
total			318.1	100.0		
at 300 rpm with 25 min						
sieve size(µm)	sieve weight(g)	Sieve+ sample(g)	weight retained(g)	Weight retained (%)	cum.wt.% passing	cum.% retained
500	483.6	521.3	37.7	11.9	88.1	11.9
250	250.7	295.9	45.2	14.2	73.9	26.1
180	278	308.7	30.7	9.7	64.3	35.7
150	241.5	272.5	31	9.8	54.5	45.5

125	276.2	315.4	39.2	12.3	42.2	57.8
100	255.5	287	31.5	9.9	32.3	67.7
90	355.5	376.8	21.3	6.7	25.6	74.4
75	287.1	320.8	33.7	10.6	14.9	85.1
pan	240.2	287.7	47.5	14.9	0.0	100.0
total			317.8	100		
At 350 rpm with 25 min						
sieve size(µm)	sieve weight(g)	Sieve+ sample(g)	weight retained(g)	Weight retained (%)	cum.wt.% passing	cum.% retained
500	483.6	496	12.4	3.9	96.1	3.9
250	250.7	274.3	23.6	7.4	88.7	11.3
180	278	291.5	13.5	4.2	84.4	15.6
150	241.5	263.1	21.6	6.8	77.6	22.4
125	276.2	314.3	38.1	12.0	65.6	34.4
100	255.5	270.5	15	4.7	60.9	39.1
90	355.5	398.1	42.6	13.4	47.5	52.5
75	287.1	342.8	55.7	17.5	30.0	70.0
pan	240.2	335.4	95.2	30.0	0.0	100.0
total			317.7	100.0		
At 450 rpm with 25 min grinding time						
sieve size(µm)	sieve weight(g)	Sieve+ sample(g)	weight retained(g)	Weight retained (%)	cum.wt.% passing	cum.% retained
500	483.6	488.9	5.3	1.7	98.3	1.7
250	250.7	256.3	5.6	1.8	96.6	3.4
180	278	304.4	26.4	8.3	88.3	11.7
150	241.5	269	27.5	8.7	79.6	20.4
125	276.2	311	34.8	11.0	68.6	31.4
100	255.5	281.2	25.7	8.1	60.6	39.4
90	355.5	378.6	23.1	7.3	53.3	46.7
75	287.1	340.8	53.7	16.9	36.4	63.6
pan	240.2	355.8	115.6	36.4	0.0	100.0
total			**317.7**			
at 550 rpm with 25 min						
sieve size(µm)	sieve weight(g)	Sieve+ sample(g)	weight retained(g)	Weight retained (%)	cum.wt.% passing	cum.% retained
500	483.6	512.9	29.3	9.2	90.8	9.2
250	250.7	300.5	49.8	15.7	75.1	24.9
180	278	314.2	36.2	11.4	63.7	36.3
150	241.5	264.1	22.6	7.1	56.6	43.4
125	276.2	327.1	50.9	16.0	40.5	59.5
100	255.5	278.6	23.1	7.3	33.3	66.7
90	355.5	373.9	18.4	5.8	27.5	72.5

75	287.1	325.6	38.5	12.1	15.3	84.7
pan	240.2	288.9	48.7	15.3	0.0	100.0
total			**317.5**	100		

product size distribution for bulk feed						
at 250 rpm with 25 min						
sieve size(µm)	sieve weight(g)	Sieve +sample(g)	weight retained(g)	Weight retained (%)	cum.wt.% passing	cum.% retained
2000	334	396.8	62.8	19.8	80.2	19.8
1400	321.8	354.2	32.4	10.2	70.0	30.0
710	290.3	328.4	38.1	12.0	58.0	42.0
500	483.6	496.7	14.8	4.7	53.4	46.6
250	250.7	278.9	28.2	8.9	44.5	55.5
180	278	297.4	19.4	6.1	38.4	61.6
150	241.5	255.3	13.8	4.3	34.1	65.9
125	276.2	289.9	13.7	4.3	29.7	70.3
90	355.5	366.8	11.3	3.6	26.2	73.8
75	287.1	332.3	33.9	10.7	15.5	84.5
pan	240.2	289.5	49.3	15.5	0.0	100.0
total			**317.7**	100.0	100.0	
at 300 rpm with 25 min						
sieve size(µm)	sieve weight(g)	Sieve+ sample(g)	weight retained(g)	Weight retained (%)	cum.wt.% passing	cum.% retained
2000	334	388.6	54.6	17.2	82.8	17.2
1400	321.8	351	29.2	9.2	73.6	26.4
710	290.3	324.4	34.1	10.7	62.9	37.1
500	483.6	498.5	14.9	4.7	58.2	41.8
250	250.7	271.8	21.1	6.6	51.5	48.5
180	278	303.7	25.7	8.1	43.5	56.5
150	241.5	255.8	14.3	4.5	38.9	61.1
125	276.2	288.9	12.7	4.0	34.9	65.1
100	255.5	263.9	8.4	2.6	32.3	67.7
90	355.5	370.1	14.6	4.6	27.7	72.3
75	287.1	322.7	35.6	11.2	16.5	83.5
-75	240.2	292.6	52.4	16.5	0.0	100.0
			317.6	**100.0**		
at 350 rpm with 25 min						
sieve size(µm)	sieve weight(g)	Sieve+ sample(g)	weight retained(g)	Weight retained (%)	cum.wt.% passing	cum.% retained
2000	334	360.2	26.2	8.7	91.3	8.7

1400	321.8	322	0.2	0.1	91.2	8.8
710	290.3	300	9.7	3.2	88.0	12.0
500	483.6	486.8	3.2	1.1	86.9	13.1
250	250.7	264.7	14	4.7	82.2	17.8
180	278	297.3	19.3	6.4	75.8	24.2
150	241.5	253.3	11.8	3.9	71.9	28.1
125	276.2	302.1	25.9	8.6	63.3	36.7
90	355.5	385.7	30.2	10.1	53.2	46.8
75	287.1	357.7	70.6	23.5	29.7	70.3
pan	240.2	329.3	89.1	29.7	0.0	100.0
			300.2	100.0		
at 450 rpm with 25 min						
sieve size(µm)	sieve weight(g)	Sieve+ sample(g)	weight retained(g)	Weight retained (%)	cum.wt.% passing	cum.% retained
500	483.6	512.62	29.02	9.2	90.8	9.2
250	250.7	268	17.3	5.5	85.4	14.6
180	278	304.2	26.2	8.3	77.1	22.9
150	241.5	256.4	14.9	4.7	72.4	27.6
125	276.2	295.7	19.5	6.2	66.2	33.8
90	355.5	368	20.5	6.5	59.7	40.3
75	287.1	319.9	32.8	10.4	49.4	50.6
pan	240.2	388.4	156.2	49.4	0.0	100.0
			316.4	100.0		
at 550 rpm with 25 min						
sieve size(µm)	sieve weight(g)	Sieve +sample(g)	weight retained(g)	Weight retained (%)	cum.wt.% passing	cum.% retained
2000	334	356.6	22.6	7.1	92.9	7.1
1400	321.8	335.6	13.8	4.3	88.5	11.5
710	290.3	350.3	20	6.3	82.3	17.7
500	483.6	518.1	34.5	10.9	71.4	28.6
250	250.7	307.7	57	17.9	53.5	46.5
180	278	308.5	30.5	9.6	43.9	56.1
150	241.5	260.8	19.3	6.1	37.8	62.2
125	276.2	302.2	26	8.2	29.6	70.4
90	355.5	371.1	15.6	4.9	24.7	75.3
75	287.1	318.2	31.1	9.8	14.9	85.1
pan	240.2	287.6	47.4	14.9	0.0	100.0